Drug Design, Development and Therapy

Dovepress
Taylor & Francis Group

Open Access Full Text Article

ORIGINAL RESEARCH

Qingre Huoxue Decoction Alleviates Atherosclerosis by Regulating Macrophage Polarization Through Exosomal miR-26a-5p

Weifeng He[1], Huanyi Zhao[2], Weiqi Xue[1], Yuan Luo[1], Mengyuan Yan[1], Junlong Li[2], Lijin Qing[2], Wei Wu[2], Zheng Jin[2]

[1]Guangzhou University of Chinese Medicine, Guangzhou, Guangdong, 510405, People's Republic of China; [2]First Affiliated Hospital of Guangzhou University of Chinese Medicine, Guangzhou, Guangdong, 510405, People's Republic of China

Correspondence: Wei Wu; Zheng Jin, Department of Cardiovascular, First Affiliated Hospital of Guangzhou University of Chinese Medicine, No. 16, Ji Chang Road, Baiyun, Guangzhou, 510405, People's Republic of China, Tel +86-020-3659-6422, Email wwhrlz@163.com; zyjinzheng@163.com

Drug Design, Development and Therapy downloaded from https://www.dovepress.com/
For personal use only.

Background: Qingre Huoxue Decoction (QRHX) is a classical Chinese herbal prescription widely used in clinical practice for the treatment of atherosclerosis (AS). Our previous study demonstrated its efficacy in stabilizing plaque and improving prognosis, as well as its ability to regulate macrophage polarization. This study aimed to further investigate the effects of QRHX on AS and explore the underlying mechanisms.

Methods: ApoE$^{-/-}$ mice were fed a high-fat diet (HFD) for 8 weeks in order to establish an AS model. Oil Red O, H&E, Masson, and IHC staining were employed to assess lipid accumulation, plaque development, collagen loss and target of the aortas tissue. ELISA was employed to measure the levels of TNF-α and IL-10 in serum. Dual luciferase reporter assay was conducted to ascertain the connection between miR-26a-5p and PTGS2 in vitro. Western blot and RT-qPCR assay were conducted to assess the NF-κB signaling pathway and macrophage polarization. The effects of miR-26a-5p were tested after transfecting miR-26a-5p over-expressive lentivirus.

Results: QRHX attenuated HFD-induced plaque progression and inflammation of AS model mice. BMDM-derived exosomes (BMDM-exo) increased miR-26a-5p and decreased PTGS2 expressions, inhibited the NF-κB signaling pathway and regulated macrophage polarization in vivo. These effects of BMDM-exo were further enhanced after QRHX intervention. Dual luciferase reporter assay results showed that miR-26a-5p directly binds to the 3'-UTR of PTGS2 mRNA and regulates the expression of PTGS2. The miR-26a-5p of BMDM-exo played a key role in macrophage polarization. After overexpression of miR-26a-5p, the NF-κB signaling pathway was inhibited and macrophages were converted from M1 to M2 in vitro.

Conclusion: QRHX can exert anti-inflammatory and plaque-stabilizing effects through exosomal miR-26a-5p via inhibiting the PTGS2/NF-κB signaling pathway and regulating macrophage phenotype from M1 to M2 polarization in AS.

Keywords: Qingre Huoxue decoction, atherosclerosis, exosomes, miR-26a-5p, macrophage polarization

Introduction

Atherosclerosis (AS) is a chronic inflammatory and abnormal lipid metabolism vascular disease characterized by the accumulation of lipids within the intimal layer of arterial walls. It affects vascular elasticity and contributes to numerous cardiovascular diseases, including myocardial infarction, hypertension, and stroke.[1] Research has demonstrated that macrophages are involved throughout the various stages of arterial plaque formation, including initiation, growth, rupture, and wound healing. Dying macrophages secrete intracellular lipid contents and tissue factors into the plaque's necrotic core, leading to increased plaque instability and triggered thrombosis.[2] Among plaque cells, macrophages exhibit strong phenotypic plasticity and polarize into pro-inflammatory M1 macrophages and anti-inflammatory M2 macrophages in response to different microenvironmental stimuli.[3,4] M1 macrophages are involved in inflammation and promote AS, whereas M2 macrophages promote tissue repair, inflammation abatement, and AS regression.[5] Macrophage-

Received: 9 August 2024
Accepted: 2 December 2024
Published: 28 December 2024

© 2024 He et al. This work is published and licensed by Dove Medical Press Limited. The full terms of this license are available at https://www.dovepress.com/terms.php and incorporate the Creative Commons Attribution – Non Commercial (unported, v3.0) License (http://creativecommons.org/licenses/by-nc/3.0/). By accessing the work you hereby accept the Terms. Non-commercial uses of the work are permitted without any further permission from Dove Medical Press Limited, provided the work is properly attributed. For permission for commercial use of this work, please see paragraphs 4.2 and 5 of our Terms (https://www.dovepress.com/terms.php).

targeted therapeutic strategies for AS have attracted considerable attention and may become a novel therapeutic objective for AS.[6,7] According to Bouchareychas and Hayde, NF-κB translocates to the nucleus where it binds to specific DNA sequences, promoting the transcription of genes involved in the inflammatory response and playing a role in macrophage M1 polarization. This process produces pro-inflammatory cytokines such as interleukin 1β (IL-1β) and tumor necrosis factor α (TNF-α), contributing to the perpetuation of the inflammatory response within atherosclerotic plaques.[8,9]

Exosomes originate from endosomes, and its ablity of carrying microRNAs (miRNAs) or siRNAs have been shown to regulate inflammatory responses and promote vascular regeneration and repair. They are involved in intercellular communication in human health and disease, including the cardiovascular system.[10] BMDM (Bone marrow-derived macrophages)-derived exosomes have been reported to modulate intercellular communication in terms of systemic and vascular inflammation in hyperlipidemic mice by delivering miRNAs.[9] These studies suggest that regulating gene expression in target cells via exosomes may be a potential approach for treating AS.[11]

There are several drug treatments for AS which have been common used in clinical settings. Statins constitute the primary treatment for AS, effectively decelerating its progression and diminishing the incidence of cardiovascular events. However, a residual risk of further vascular events persists, alongside potential side effects such as hepatic and renal damage, which may adversely impact patient adherence to the treatment.[12] Ezetimibe is associated with fewer adverse effects and reduces low-density lipoprotein cholesterol (LDL-C) levels by 18% to 20%. It can be co-administered with statins for patients whose LDL-C levels remain suboptimal after moderate-intensity statin therapy, further mitigating the risk of cardiovascular events.[13,14] Proprotein convertase subtilisin/kexin type 9 (PCSK9) inhibition, such as evolocumab and alirocumab, show excellent LDL-C lowering effects, along with good tolerability and safety profiles.[15,16] However, their high cost is a limiting factor.[15,16] Xuezhikang, a partially purified extract of red yeast rice, has demonstrated efficacy in reducing LDL-C levels and has shown clinical benefits in secondary prevention studies conducted within the Chinese population. It is associated with decreased mortality and a reduction in cardiovascular events among individuals with coronary heart disease while exhibiting minimal adverse effects.[17,18] Considering the side effects, cost, and potency of existing drugs, an increasing number of researchers have been seeking safer and more effective alternatives in recent years.

Traditional Chinese Medicine (TCM) is increasingly utilized in the treatment of cardiovascular diseases due to its multi-targeting characteristics and cardioprotective effects.[19–21] Qingre Huoxue Decoction (QRHX) is a TCM compound. QRHX has been shown to stabilize plaques, improve prognosis, reduce the incidence of recurrent ischemic events and adverse cardiovascular outcomes, and improve clinical symptoms and quality of life in patients with myocardial infarction.[22–24] In addition, QRHX is readily accessible, straightforward to process, economically viable, and could alleviate symptoms while addressing some limitations associated with chemical pharmaceuticals.[22–24] QRHX is composed of seven Chinese herbs: Scutellaria baicalensis Georgi (Lamiaceae, HQ), Salvia miltiorrhiza Bunge (Lamiaceae, DS), Paeonia veitchii Lynch (Paeoniaceae, CS), Ligusticum chuanxiong S.H.Qiu, Y.Q.Zeng, K.Y.Pan, Y.C.Tang & J.M. Xu (Apiaceae, CX), Dalbergia odorifera T.C.Chen (Fabaceae, JX), Carthamus tinctorius L (Asteraceae, HH), and Ilex pubescens Hook. and Arn (Aquifoliaceae, MDQ). According to TCM theory, heat toxin is a pathogenic factor that causes excessive pathological changes of hot and yang nature, often leading to the damage in blood vessels or slowing blood flow.[25] Heat toxin is responsible for the development of AS.[26] Inflammation and heat toxin are closely related.[27,28] Therefore, QRHX consists of herbs that have the ability of clearing heat, removing toxins, activating blood circulation, and possessing anti-inflammatory properties.[25,27,29] These herbs of QRHX are regarded as relatively safe, with no significant toxicity reported under reasonable use, when used according to the recommended doses specified in the Chinese Pharmacopoeia.[30] In prior clinical investigations, no abnormalities in hepatic or renal function were observed following the use of QRHX.[23,29] Furthermore, QRHX was found to mitigate contrast-induced renal impairment in post-PCI patients.[31]

Previous studies suggested that QRHX contains 68 compounds (54 in positive and 24 in negative ion mode, 10 duplicates. Table 1). Baicalin and salvianolic acid B were the highest in the QRHX examined by the ultra-performance liquid chromatography-mass spectrometry (UPLC-MS) analysis.[32] Studies have shown that baicalin and salvianolic acid B have no significant acute or chronic toxicity.[33–36] Furthermore, baicalein and salvianolic acid B have been shown to alleviate AS and are closely related to NF-κB signaling pathway and macrophage polarization.[37–42] Additionally, the

Table 1 The 68 Compounds of QRHX

NO.	RT (min)	Formula	Target Mass	Diff (ppm)	Identification
1	0.307	$C_{17}H_{27}NO_3$	293.1991	1.67	Nobilonine
2	0.557	$C_5H_7NO_3$	129.0426	−2.53	Pyroglutamic acid
3	0.607	$C_{40}H_{30}O_{24}$	894.1127	−0.46	Diellagic acid rhamnoside (1-->4)glucopyranoside
4	0.607	$C_{41}H_{32}O_{26}$	940.1182	−0.44	1,2,3,4,6-Pentagalloylglucose
5	0.607	$C_7H_6O_5$	170.0215	−3.06	Gallic acid
6	0.623	$C_{28}H_{24}O_{16}$	616.1064	1.99	Desmanthin 2
7	0.623	$C_{36}H_{30}O_{16}$	718.1534	−1.47	Fukugiside
8	0.64	$C_{26}H_{22}O_{10}$	494.1213	−0.74	Salvianolic acid A
9	0.723	$C_{19}H_{24}O_6$	348.1573	0.33	9-Hydroxyglabratolide
10	0.79	$C_{11}H_{14}O_3$	194.0943	1.08	2-Methoxy-4-(3-methoxy-1-propenyl)-phenol
11	0.806	$C_{18}H_{34}O_5$	330.2406	2.45	Sanleng acid
12	0.823	$C_{21}H_{36}N_2O$	332.2828	−3.21	Holarrhimine
13	0.823	$C_{17}H_{32}O_3$	284.2351	2.85	Muricatacin
14	0.823	$C_{17}H_{28}NO_2$	278.212	1.03	N-Methyldendrobium
15	0.823	$C_{18}H_{22}O_4$	302.1518	2.43	Arnebinone
16	1.022	$C_{12}H_{22}O_2$	198.162	−2.35	cis-4-Dodecenoic acid
17	1.339	$C_{21}H_{33}NO$	315.2562	−0.23	Holadysine
18	1.455	$C_{20}H_{27}NO$	297.2093	0.18	Spirasine IV
19	2.004	$C_{19}H_{27}NO$	285.2093	−0.8	1-Methyl-2-nonyl-4(1H)-quinolone
20	2.985	$C_{36}H_{38}O_8$	598.2567	−0.08	Tinyatoxin
21	3.235	$C_{22}H_{33}NO$	327.2562	2.45	1-Methyl-2-dodecyl-4-(1H)-quinolone
22	4.05	$C_{37}H_{40}O_9$	628.2672	0.34	Resiniferotoxin
23	4.832	$C_{30}H_{28}O_8$	516.1784	2.65	Rottlerin
24	5.198	$C_{30}H_{28}O_8$	516.1784	2.15	Rottlerin
25	0.604	$C_5H_{10}O$	86.0732	4.94	1-Penten-3-ol
26	0.612	$C_6H_{14}O_2$	118.0994	0.87	Acetal
27	0.612	$C_{12}H_{22}O_{11}$	342.1162	−2.12	Cellobiose
28	0.621	$C_{24}H_{42}O_{21}$	666.2219	−1.17	Isolychnose
29	0.687	C_9H_{12}	120.0939	0.11	1,2,3-Trimethylbenzene
30	0.945	$C_6H_5NO_2$	123.032	2.5	Nicotinic acid
31	1.145	$C_7H_6O_3$	138.0317	1.73	3,4-Dihydroxybenzyl aldehyde
32	1.427	$C_{10}H_{12}O_4$	196.0736	−0.09	2,4-Dihydroxy-6-methoxy-3- methylacetophenone
33	1.569	$C_8H_6O_3$	150.0317	0.04	Piperonal
34	1.868	$C_{13}H_{11}N$	181.0892	−2.55	3-Methylcarbazole
35	1.877	$C_9H_8O_3$	164.0473	−4.65	Coumarinic acid
36	1.877	$C_{13}H_8$	164.0626	−2.82	1,11-Tridecadiene-3,5,7,9-tetrayne
37	2.093	$C_{23}H_{28}O_{11}$	480.1632	−2.27	Albiflorin R1
38	2.093	$C_{10}H_{12}O_4$	196.0736	−3.42	2,4-Dihydroxy-6-methoxy-3- methylacetophenone
39	2.226	$C_5H_{10}O$	86.0732	0.59	1-Penten-3-ol
40	2.243	$C_{10}H_8O_4$	192.0423	−0.63	6-Methoxy-7-hydroxycoumarin
41	2.326	$C_{26}H_{30}O_{14}$	566.1636	−1.75	Angustioside
42	2.342	$C_8H_{10}O$	122.0732	0.06	2,3-Dicresol
43	2.342	$C_{10}H_{10}O_3$	178.063	0.23	Coniferyl aldehyde
44	2.351	$C_{10}H_8O_2$	160.0524	−0.19	1,2-Hydronaphthoquinone
45	2.475	$C_{34}H_{46}O_{18}$	742.2684	0.91	(+)-Syringaresinol-di-O-beta-Dglucoside
46	2.642	$C_9H_{10}O_4$	182.0579	−3.47	Jacaranone
47	2.658	$C_9H_{12}O_3$	168.0786	−1.31	2-Methoxy-2-(4'-hydroxyphenyl)ethanol
48	2.767	$C_{26}H_{26}O_{12}$	530.1424	−0.57	Macranthoin F
49	2.941	$C_{11}H_{10}O_5$	222.0528	−1.75	5,6-Dimethoxy-7-hydroxycoumarin

(*Continued*)

https://doi.org/10.2147/DDDT.S487476

Table 1 (Continued).

NO.	RT (min)	Formula	Target Mass	Diff (ppm)	Identification
50	2.966	$C_{21}H_{20}O_9$	416.1107	−0.8	Apigenin-5-rhamnoside
51	2.975	$C_{12}H_{16}O_3$	208.1099	−2.87	1-Allyl-2,4,5-trimethoxy-benzene
52	3.166	$C_8H_8O_2$	136.0524	−2.29	4-Methyl salicylaldehyde
53	3.241	$C_{10}H_{20}O$	156.1514	−4.07	1-Methyl-3-isopropoxy cyclohexane
54	3.59	$C_{10}H_8O_3$	176.0473	−3.72	6-Hydroxy-7-methylesculetin
55	3.607	$C_8H_8O_3$	152.0473	2.22	2,4-Dihydroxyacetophenone
56	3.665	$C_{14}H_{14}O_5$	262.0841	−0.5	Celereoin
57	3.806	$C_8H_8O_3$	152.0473	1	2,4-Dihydroxyacetophenone
58	3.84	$C_{16}H_{16}O_5$	288.0998	−1.93	5-Hydroxymethyl-6-endo-3'-methoxy-4'-hydroxyphenyl-8-oxabicyclo[3,2,1]-oct-3-en-2-one
59	3.856	$C_8H_8O_3$	152.0473	−1.9	2,4-Dihydroxyacetophenone
60	3.989	$C_{10}H_{26}N_4$	202.2158	−1.07	Spermine
61	4.189	$C_9H_{10}O_3$	166.063	−3.86	2,4-Dimethoxybenzaldehyde
62	4.189	$C_8H_8O_3$	152.0473	−1.88	2,4-Dihydroxyacetophenone
63	4.264	$C_9H_{10}O_3$	166.063	−3.1	2,4-Dimethoxybenzaldehyde
64	4.355	$C_9H_{10}O_3$	166.063	0.11	2,4-Dimethoxybenzaldehyde
65	4.447	$C_9H_6O_3$	162.0317	−3.06	3-Hydroxycoumarin
66	4.538	$C_9H_{16}O$	140.1201	−1.59	(E)-2-Nonenal
67	4.538	$C_8H_8O_3$	152.0473	−0.41	2,4-Dihydroxyacetophenone
68	4.555	$C_{18}H_{16}O_7$	344.0896	−0.79	3',4'-Dihydroxywogonin
69	4.597	$C_8H_8O_2$	136.0524	2.21	4-Methyl salicylaldehyde
70	4.73	$C_{10}H_{18}O_2$	170.1307	−4.61	6alpha-Methyl-2alpha,6betadihydroxymethylbicyclo[3.1.1]heptane
71	4.996	$C_{19}H_{18}O_5$	326.1154	−0.11	2,5-Dimethoxy-4-hydroxy-[2″,3″:7,8]-furanoflavan
72	5.037	$C_{12}H_{14}O$	174.1045	−3.06	4,7-Dimethyl-1-tetralone
73	5.046	$C_8H_8O_2$	136.0524	−1.12	4-Methyl salicylaldehyde
74	6.019	$C_{16}H_{12}N_2O_2$	264.0899	−3.56	Nauclefidine
75	6.718	$C_{30}H_{48}$	408.3756	1.61	Neohopadiene
76	11.193	$C_{12}H_{18}O_2$	194.1307	−1.7	(+)-Myrtenyl acetate
77	12.1	$C_5H_{11}NO_2$	117.079	−1.16	Betaine
78	12.1	$C_5H_8O_2$	100.0524	−1.35	Tiglic acid

results of previous RNA sequencing studies of in vivo and vitro samples in our team indicated that the NF-κB signaling pathway, TNF signaling pathway, and IL-17 signaling pathway were most significantly enriched after QRHX intervention.[24] The previous literature show that NF-κB signaling pathway plays a key role in regulating macrophage polarization.[43,44] Finally, we chose the NF-κB signaling pathway and demonstrated that NF-κB signaling pathway was the target pathway for QRHX-induced M2 polarization.[24] Simultaneously, we conducted a screening of 16 target genes within the NF-κB signaling pathway and ultimately identified PTGS2 as a target of QRHX intervention in AS via NF-κB signaling pathway.[24] Using literature search and TargetScan (https://www.targetscan.org/vert_80/), we identified miR-26a-5p as an upstream target of PTGS2. Multiple studies have showed a significant link between the expression levels of miR-26a-5p and the development of cardiovascular disease. MiR-26a-5p protects cardiomyocytes from hypoxia/reoxygenation-induced injury,[45] prevents apoptosis,[46] and guards against myocardial ischemia/reperfusion injury.[47] These effects help to reduce chronic inflammation,[48–50] and ameliorate hypertrophied myocardium[51] by inhibiting the NF-κB signaling pathway. Mompeon et al found in patients experiencing non-ST-segment elevation myocardial infarction (NSTEMI), the expression of miR-26a-5p exhibited an inverse correlation with serum concentrations of the pro-inflammatory cytokine TNF-α.[52] In patients diagnosed with ST-segment elevation myocardial infarction (STEMI), a decrease in miR-26a-5p levels has been linked to an increased incidence of adverse cardiovascular events.[53] We hypothesize that miR-26a-5p may play anti-inflammatory, antioxidant, and anti-apoptotic roles in the early stages of AS

development and could improve prognosis by being anti-inflammatory after disease progression or even in STEMI. Additionally, miR-26a regulates macrophage polarization[54] and promotes the shift from M1 to M2 macrophages while inhibiting the production of inflammatory factors.[55] Therefore, we hypothesized that QRHX may exert anti-AS effects by influencing macrophage polarization phenotype through exosomal miR-26a-5p via inhibiting the PTGS2/NF-κB signaling pathway.

Materials and Methods

Drug Preparation

The herbs were procured from the Chinese herbal pharmacy of the First Affiliated Hospital of Guangzhou University of Traditional Chinese Medicine. The seven herbs, HQ, MDQ, DS, JX, HH, CX, and CS, were weighed and mixed in the ratio of 3:6:6:2:2:2:3 according to the original prescription.[24,29] The herbs are soaked in 720 mL of water to ensure that all herbs are fully submerged. Then, soak for 30 minutes to promote the extraction, followed by sustained boiling for 1 hour. Afterward, pour out the filtrate, and repeat the process with another 720 mL of water, boiling for an additional hour. And the two medicinal liquids were combined. The mixture of QRHX was centrifuged at a speed of 5000 revolutions per minute (rpm) and a temperature of 4 °C for 15 minutes. The supernatant was collected and subjected to vacuum freeze-drying at −80 °C for 72 hours to produce lyophilized powder.[24]

Animals and Experimental Design

This study was approved by the Ethics Committee for the First Affiliated Hospital of Guangzhou University of Traditional Chinese Medicine (GZTCMF1-2021076). All animal experiments were conducted in accordance with the guidelines outlined in the National Institutes of Health Guide for the Care and Use of Laboratory Animals. The animals were housed at a temperature of 23 ± 1 °C under a 12-hour light-dark cycle and were provided with standard chow and water. Eighty $ApoE^{-/-}$ mice (C57BL/6J background, weeks: 8 ± 1, males, body weight: 18g-22g) were purchased from Jiangsu Jicui Pharmachem Biotechnology Co. and housed in the SPF-grade animal laboratory of the First Affiliated Hospital of Guangzhou University of Traditional Chinese Medicine. The mice were split into two batches for the experiment, the first batch of fifty mice was divided into five groups at random (randomized numerical table method[56]) after seven days of adaptive feeding (n=10): the control group (NC group), the model group (MOD group), and three groups of QRHX: the low-dose group (QRHX-L group, 7.5 g/kg/d), the medium-dose group (QRHX-M group, 15 g/kg/d), and high dose group (QRHX-H group, 30 g/kg/d). The doses of QRHX (7.5 g/kg/d, 15 g/kg/d, 30 g/kg/d) were established based on a review of existing literature, equivalent to 1, 2, and 4 times the human drug dose.[24,57] The doses of QRHX were established after reviewing existing literature, ensuring they fall within a safe and effective range for the medication.[24] The second batch of thirty mice were randomly divided into three groups (randomized numerical table method[56]) of ten animals each (n=10) after seven days of acclimatization feeding: blank group (CON group, 200 μL PBS injected in the tail vein), control group (BMDM-exo group, BMDM-derived exosomes, 10^{10}/each, dissolution in 200 μL PBS injected in the tail vein), and treatment group (BMDM-QRHX-exo group, BMDM-derived exosomes of QRHX-intervened, 10^{10}/each, dissolution in 200 μL PBS injected in the tail vein). All groups except the NC group were fed a high-fat diet (HFD) to induce AS and mice were monitored weekly for body weight. The composition of the HFD was as follows: 21% fat, 0.15% cholesterol, 15.5% protein, and 62% standard feed. This HFD was procured from the Guangdong Medical Laboratory Animal Center. The intervention was started after week 8, and after 8 weeks of intervention, the mice were anesthetized by giving an intraperitoneal injection of 1% sodium pentobarbital at a concentration of 50 mg/kg. Specimens were collected by dissecting the thorax and abdomen, and blood was collected from the abdominal aorta.

Reagents and Antibodies

GW4869 was purchased from MCE (HY-19363, Shanghai, China). Puromycin solution was purchased from Biosharp (BL528A, Hefei, China). Cell culture chambers were purchased from LABSELECT (14111-D, Hefei, China). The H&E staining kit was purchased from Leagene (DH0006; Beijing, China). Anti-MOMA-2 (Abcam, ab33451, 1:2000), iNOS

(Abcam, ab178945, 1: 1000), GAPDH (Abcam, ab181602, 1:10,000), and HRP rabbit anti-mouse IgG (Abcam, ab6728, 1:5000), Arg-1 (CST, 93668S, 1: 1000), p65 (Abcam, ab32536, 1:1000) and p50 (ThermoFisher, MA5-32911, 1:1000).

Enzyme-Linked Immunosorbent Assay (ELISA)

ELISA kits were employed to measure the levels of serum inflammatory factors TNF-α (MM-0132M1, MEIMIAN, Jiangsu, China) and IL-10 (MM-0176M1, MEIMIAN, Jiangsu, China) in mice. As directed by the kit instructions, various concentrations of samples and standards were added. Enzyme reagents were introduced to all wells except the blank wells before incubation for one hour at 37 °C in a thermostat. After that, the wells were properly cleaned five times. Substrate solutions A and B were sequentially added, and the mixture was incubated at 37 °C for 15 minutes without exposure to light. After adding the stop solution, the optical density (OD) at 450 nm for each sample was ascertained.

Histology

The entire aorta was carefully dissected and longitudinally opened to expose the luminal surface. Subsequently, the tissue was stained with an Oil Red O working solution, a lipid-specific dye, to quantitatively and qualitatively assess lipid deposition. Images were taken with a Canon digital camera. After aortic tissues were embedded in paraffin and fixed with 4% paraformaldehyde, they were microtomed into 4 μm slices. H&E staining was used to assess plaque area, Masson staining to assess collagen fiber content, and immunohistochemistry to detect the levels of α-smooth muscle actin (α-SMA), and the monocyte/macrophage marker MOMA-2. Sections were scanned using a digital pathology section scanning system (Pannoramic MIDI, 3D HISTEC), images were collected, and images were analyzed with Image J. The results of this study were used to determine the levels of collagen fibers, smooth muscle cells (SMCs), and macrophages.

Cells Culture

BMDMs were isolated and cultured from the tibia and femur of C57BL/6J mice (6–8 weeks old).[58] Following the removal of the tibia and femur ends, aseptic conditions were maintained by flushing the medullary cavity with a syringe before the cells were collected and resuspended into culture flasks. Dulbecco's Modified Eagle Medium (DMEM) supplemented with 10% fetal bovine serum, 1% penicillin-streptomycin, and 15% L929 supernatant was used to culture BMDMs for seven days.[59] The medium was changed on days three, five, and seven. After seven days, the culture media was replaced once on days three, five, and seven for use in later studies. L929 cells (1.2×10^6) were seeded into 100 mm culture dishes with 10 mL of DMEM complete medium, and the supernatant was collected after 7 days. The supernatant was centrifuged to remove cellular debris, filtered through a strainer, and stored at −80 °C for future use. Mouse fibroblast cell line L929 was purchased from Wuhan Punosai Life Science and Technology Co., Ltd (No. CL-0137). 293T cells were purchased from Wuhan Xavier Life Science and Technology Co., Ltd (No. STCC10301G-1). Mouse monocyte-macrophage leukemia cell line RAW264.7 was purchased from Wuhan Punosai Life Science and Technology Co., Ltd, item no. CL-0190. All cells were cultivated at 37 °C with 5% CO2 in DMEM supplemented with 10% fetal bovine serum and 1% penicillin-streptomycin.

Cell Counting Kit-8 Assay

BMDMs (1×10^4 cells/well) were injected in 96-well plates for the CCK-8 experiment. After that, the cells were exposed to various doses of QRHX (0, 20, 40, 80, 100, 150, 200, and 400 μg/mL) for 24 hours. Following the removal of the medium and a PBS wash, 10 μL of CCK-8 solution per well was added, and the plates were incubated at 37 °C for 2h. An enzyme meter was then used to determine the OD value at 450 nm.

Isolation and Characterization of exosomes

After BMDMs were cultured in the exosome-free medium for 72 h, cell supernatants were collected, and exosomes were extracted using the differential centrifuge method.[60] Sequentially, the cells were centrifuged at 400 g, 4 °C, for 10 min; 2000 g, 4 °C, for 10 min; 10,000 g, 4 °C, for 30 min; and 100,000 g, 4 °C, for 70 min. Ultimately, PBS was used to resuspend the final precipitate (exosomes), and they were centrifuged once more for 70 minutes at 100,000 g and 4 °C. After dissolving the

exosomes in 200 μL of 1× PBS, they were stored at −80 °C. Transmission electron microscopy (Hitachi, HT7700) was used to assess the morphology of BMDM-derived exosomes. The purified exosomes were resuspended with 50μL of 2% paraformaldehyde, followed by a dropwise addition of 5 μL of the resuspension solution on a carbon nanotube-coated grid, and thoroughly adsorbed for 20 minutes in a dry setting. A filter paper was used to blot out the liquid, and a dropwise addition of 15 μL of a dipoxyuranum oxalate staining solution with a concentration of 2% was applied to it for 2 min. The grid was then washed with purified water, dried, and placed under a nano TEM for observation and photography. A 500 ng/mL dilution of the collected exosomes was used to prevent inter-particle interactions. The size and number of exosomes were studied by a nanosized particle tracking analyzer (Particle Metrix, ZetaView).

Western Blot

Mouse aorta, RAW264.7 cells, and exosomal proteins were extracted using RIPA lysis buffer and a protease inhibitor mixture. Total proteins were quantified by the BCA method, and Western blot was performed on 10% SDS-PAGE and 0.22 μm PVDF membranes. The intensity of bands was analyzed by Image J software.

Quantitative Reverse Transcription PCR (RT-qPCR)

Gene expression levels were quantified by RT-qPCR. mRNA was collected using the Universal RNA Extraction Kit (AG, AG21017, Hunan, China) and transformed into cDNA using the Reverse Transcription Reagent Premix (AG, AG11706, Hunan, China). miRNA was collected by the miRNA Extraction Kit (AG, A5A1770, Hunan, China) and transformed into cDNA using SYBR Green (AG, AG11701, China). and transformed into cDNA using miRNA First Strand cDNA Kit (AG, AG11716, China). The mRNA was detected by RT-qPCR using SYBR Green (AG, AG11701, China) with Applied Biosystems Quant Studio 5 (Thermo, USA), specific primers for RT-qPCR detection. The relative gene expression was determined using the $2^{-\Delta\Delta}$Ct technique, with mRNA chosen as the loading control for GAPDH and miRNA selected as the loading control for U6. Three iterations of this experiment were conducted. Table 2 provides a summary of the primer sequences employed.

Transfection of Cells

After BMDMs were transfected with lentivirus containing miR-26a-5p mimic, inhibitor, or empty vector virus (GV369/GV691; Genechem, Shanghai, China, MOI=80), the expression of miR-26a-5p was detected by RT-qPCR. Using miR-26a-5p mimic and PTGS2 inhibitor lentivirus or an empty vector virus (GV369/GV493; Genechem, Shanghai, China, MOI=50) transfected into RAW264.7 cells, miR-26a-5p and PTGS2 expression was assessed via RT-qPCR. Both transfections were performed using the transfection reagent HiTransG A (REVG004; Genechem, Shanghai, China).

Luciferase Reporter Assay

The wild-type (WT) PTGS2-3'UTR and mutant (MUT) PTGS2-3'UTR were inserted into the GV272 vector (SV40-firefly luciferase-MCS) through the XbaI cleavage site. The Renilla plasmid was transfected according to the manufacturer's instructions using Lipofectamine 3000 (Invitrogen) (TK promoter-Renilla luciferase). miR-26a-5p mimic or negative control was cotransfected into 293T cells. Cells were taken after 48 hours and subjected to analysis using the Dual-Luciferase Reporter Assay System (Promega, E1910, USA) and a multifunctional enzyme labeling instrument to measure the luciferase activities

Table 2 Primers List

Gene	Forward Primer	Reverse Primer
GAPDH	GGTTGTCTCCTGCGACTTCA	TGGTCCAGGGTTTCTTACTCC
iNOS	GTTCTCAGCCCAACAATACAAGA	GTGGACGGGTCGATGTCAC
Arg-1	CTCCAAGCCAAAGTCCTTAGAG	AGGAGCTGTCATTAGGGACATC
PTGS2	CATCCCCTTCCTGCGAAGTT	GGCCCTGGTGTAGTAGGAGA
U6	CTCGCTTCGGCAGCACAT	AACGCTTCACGAATTTGCGT
miR-26a-5p	GGCAAGTAATCCAGGATAGGCT	/

https://doi.org/10.2147/DDDT.S487476

of firefly and Renilla luciferases. The results of quantitatively comparing these two luciferase activities reflected the regulatory effects of miRNAs on target genes, normalized by the ratio of Renilla to Firefly luciferase signals.

Statistics

The statistical software SPSS 25.0 was used for data processing and analysis in the study. The data were first tested for normal distribution, and measures that conformed to normality were described using mean ± standard deviation (x ± s). After that, the variance alignment test was performed; when the variance was aligned, the data with the number of groups of two groups were compared between the two groups using the Independent Samples *t*-test; when the number of groups of three or more groups was aligned, the comparison between the groups was performed using the one-way ANOVA, and the two-by-two comparisons between the groups were performed using the Bonferroni correction; when the variance was not aligned, Dunnett's T3 method was used for comparison between groups. $P < 0.05$ was used as the significance level of the test.

Results

Characterization and miR-26a-5p Expression of BMDM-Derived Exosomes

Exosomes were meticulously isolated from the supernatant of BMDMs utilizing a well-established protocol involving continuous differential centrifugation followed by ultracentrifugation. This multi-step centrifugation process is designed to sequentially remove cells, debris, and larger vesicles, thereby enriching the exosome fraction. Electron microscopy analysis revealed exosomes with distinct membrane boundaries, exhibiting saucer-shaped or cup-like structures of varying sizes (Figure 1A). Western blot confirmed the presence of exosome marker proteins CD63 and TSG101

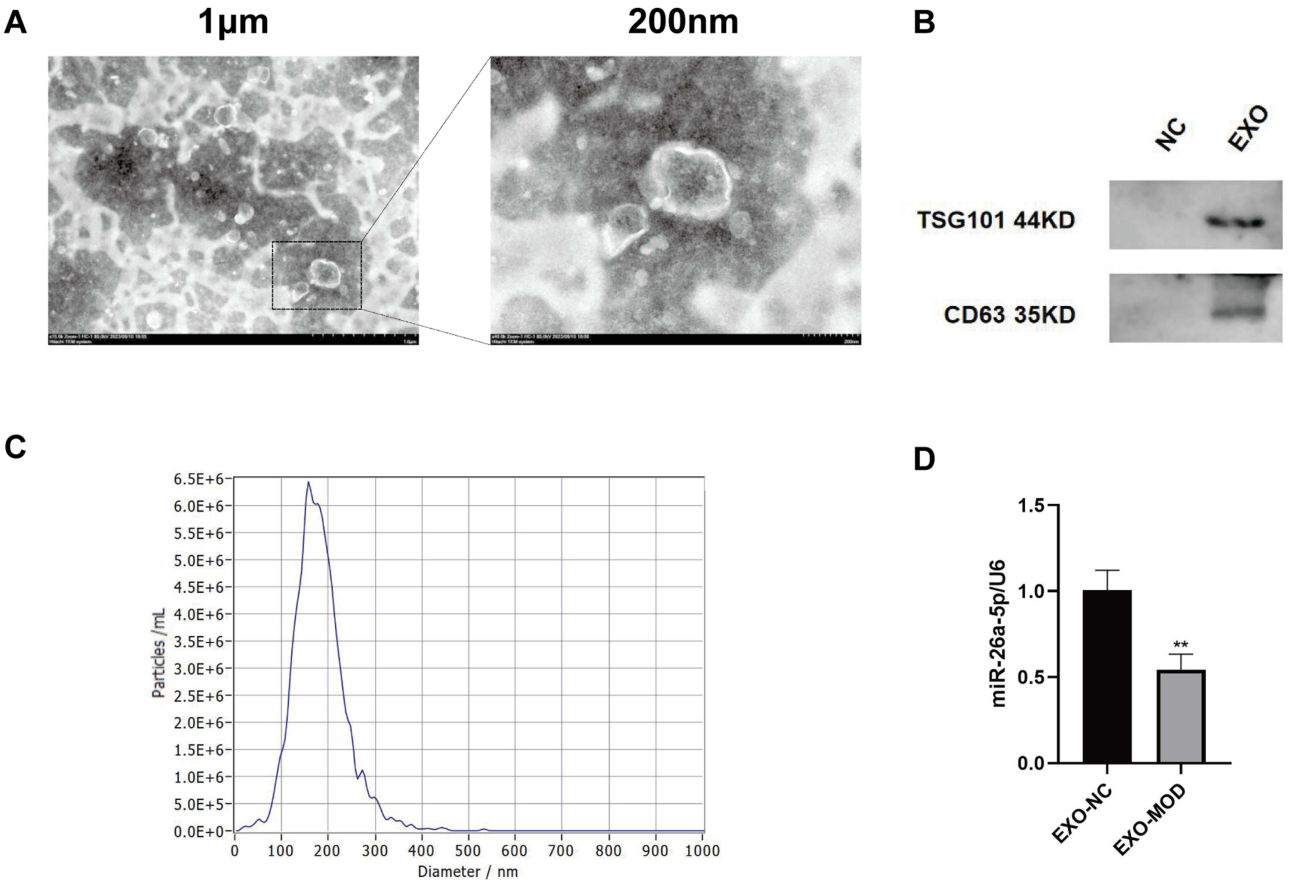

Figure 1 Characterization and miR-26a-5p expression of BMDM-derived exosomes. (**A**) Representative images of BMDM-derived exosomes. Scale bar: 1μm (left) and 200nm (right). (**B**) Exosomes were validated by assessing exosomal marker proteins CD63 and TSG101 (n=5). (**C**) Size distribution of BMDM-derived exosomes by Nanoparticle Tracking Analysis. (**D**) Expression of miR-26a-5p in exosomes isolated from different sources of BMDMs (n=5). NC: dying cell debris from BMDM cells supernatant; EXO: BMDM-derived exosomes; EXO-NC: BMDM-exo of C57BL/6J mice; EXO-MOD: BMDM-exo of AS model mice. Data were presented as mean ± standard deviation (x ± s) in an Independent Samples *t*-test. **p<0.01 vs EXO-NC group.

(Figure 1B). Nanoparticle tracking analysis indicated that the exosomes displayed a single peak at 161.6 nm with a concentration of 1.5×10^8 particles/mL (Figure 1C). RT-qPCR results showed that, compared with the EXO-MOD group, the EXO-NC group had higher expression of exosomal miR-26a-5p (Figure 1D).

QRHX Attenuated Atherosclerosis in ApoE$^{-/-}$ Mice

As shown in Figure 2A, at eight weeks of HFD-fed induction, the body weights of mice in the MOD and QRHX groups were significantly higher than those in the NC group. Following eight weeks of QRHX intervention, the body weights of mice in the three different dose groups of QRHX were lower than those in the MOD group, suggesting that QRHX reduces the weight gain induced by a high-fat diet. The levels of inflammatory factors TNF-α and IL-10 were detected by ELISA. High-fat diet (HFD) induced a severe inflammatory response, evidenced by a upward of serum TNF-α and a downward of IL-10 (Figure 2D). Compared with the MOD group, TNF-α levels were decreased and IL-10 levels were increased in both the QRHX-M and QRHX-H groups. Furthermore, the therapeutic efficacy of QRHX was more pronounced in the QRHX-H group compared to the QRHX-M and QRHX-L groups. These results suggest a dose-dependent anti-inflammatory effect of QRHX, with higher doses yielding greater reductions in pro-inflammatory cytokines and increases in anti-inflammatory cytokines. The results of oil red O staining of the entire aorta showed that the lipid deposition in the MOD group was more severe than that in the NC group, with an increased area of oil red O staining. After QRHX intervention, lipid deposition decreased with the increase of the administered dose (Figure 2B and E). H&E staining of cross-sections of the mouse aorta showed no obvious plaque formation in the aorta of the NC group, with smooth intima, no hyperplasia, and no obvious abnormality in the middle layer. In the MOD group, there was an increase in plaque formation, thickening of the intima, and deposition of foam cells, sedimentary lipids, cholesterol crystals, and necrotic substances in the plaques, with a visible and obvious fibrous cap. The area of plaques decreased after treatment with the middle and high dose of QRHX (Figure 2C and F), indicating that QRHX had a plaque-shrinking effect. In advanced AS lesions, SMCs contribute to the thickening of the plaque fibrous cap, thereby enhancing plaque stability. Therefore, IHC was used to quantitatively and qualitatively assess the presence of α-SMA within the plaque, providing critical insights into the cellular composition and potential functional implications within the plaque micro-environment. The results indicated a reduction in α-SMA content in the MOD group compared to the CON group. Conversely, an increase in α-SMA content was observed in the QRHX-M and QRHX-H group compared to the MOD group (Figure 2C and F). These findings suggest a differential modulation of α-SMA expression across the experimental groups, indicating that the middle and high dose of QRHX had a stabilizing effect on plaques.

QRHX Regulated Macrophage Polarization

Macrophage phenotypic differentiation and inflammatory state are intricately linked. In this study, we employed Western blot and RT-qPCR to evaluate the expression of M1 and M2 macrophage polarization phenotypes in vascular plaques of ApoE$^{-/-}$ mice and RAW264.7 cells. In the in vivo experiments, Western blot analyses suggested that iNOS expression was elevated and Arg-1 expression was reduced in the MOD group compared with the NC group. Conversely, the QRHX-H group demonstrated a decrease in iNOS expression, accompanied by a concomitant increase in Arg-1 expression in RT-qPCR analyses (Figure 3A and B). RT-qPCR analyses suggested that iNOS expression was elevated and Arg-1 expression was reduced in the MOD group compared with the NC group. Then, the QRHX demonstrated a dose-dependently decrease in iNOS expression, accompanied by a concomitant increase in Arg-1 expression (Figure 3C). These alterations in iNOS and Arg-1 levels suggest a shift towards an anti-inflammatory phenotype, potentially elucidating the underlying mechanisms of QRHX-mediated therapeutic effects. In the in vitro experiments, we assessed the viability of BMDM at different doses of QRHX (Figure 3D) and selected 200 μg/mL for subsequent experiments. Results of RAW264.7 cells, co-cultured with BMDM, demonstrated decreased iNOS gene expression and increased Arg-1 gene expression (Figure 3E). These effects were further amplified when BMDM were co-cultured with RAW264.7 cells following QRHX intervention (Figure 3E).

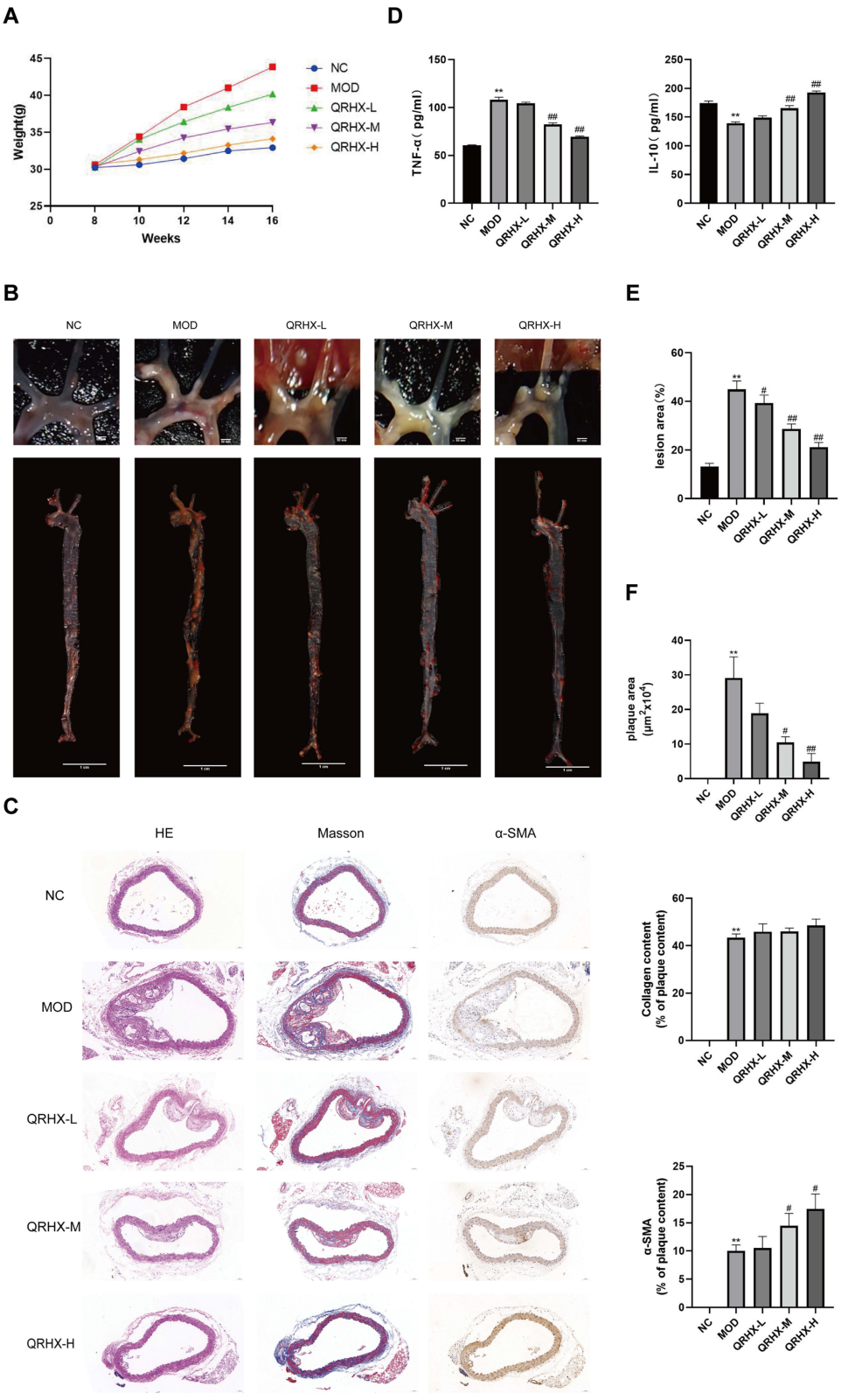

Figure 2 QRHX attenuated atherosclerosis in HFD-fed ApoE$^{-/-}$ mice. (**A**) Body weights of ApoE$^{-/-}$ mice (n=10). 0 to 8 weeks: HFD induction; 9 to 16 weeks: HFD induction, QRHX intervention. (**B** and **E**) The oil red O staining on entire aorta of ApoE$^{-/-}$ mice. The ratio is the relative area of lipid deposition staining area to the total aortic area (n=5). (**C** and **F**) H&E, Masson, and α-SMA staining of ApoE$^{-/-}$ mice. For Masson and α-SMA staining, the ratio is the relative area of the stained area within the plaque to the total area of the plaque (n=5). (**D**) ELISA for serum levels of TNF-α and IL-10 (n=10). NC: normal diet; Model: high-fat diet; QRHX-L: QRHX low-dose group (HFD + 7.5 g/kg/d QRHX); QRHX-M: QRHX medium-dose group (HFD + 15 g/kg/d QRHX); QRHX-H: QRHX high-dose group (HFD + 30 g/kg/d QRHX). Data were presented as mean ± standard deviation (x ± s) in one-way ANOVA. **p<0.01 vs NC group; $^{\#}$p<0.05, $^{\#\#}$p<0.01 vs MOD group.

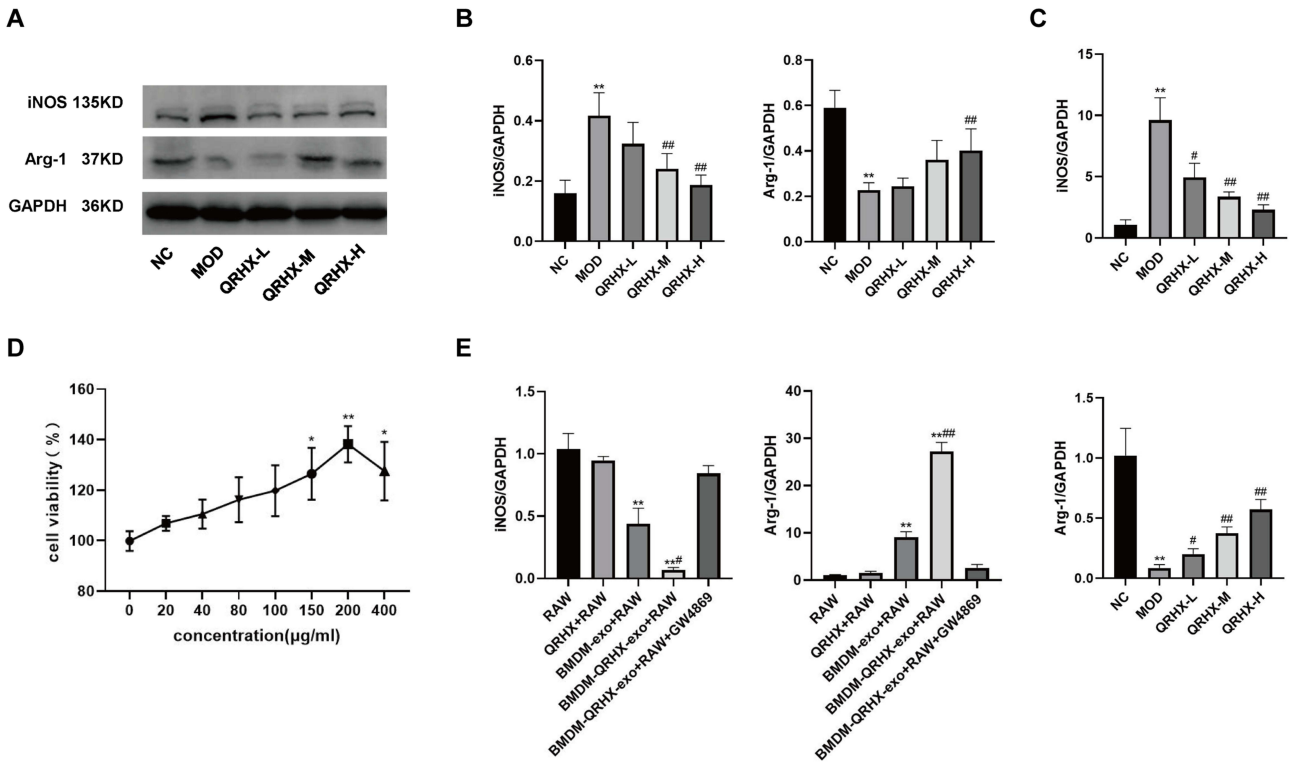

Figure 3 Effect of QRHX on macrophage polarization in ApoE$^{-/-}$ mice and miR-26a-5p of BMDM-derived exosomes in RAW264.7. (**A** and **B**) Western blot analysis was conducted to evaluate the expression of iNOS and Arg-1 in the aortas of ApoE$^{-/-}$ mice (n=5). (**C** and **E**) RT-PCR was performed to assess the gene expression levels of iNOS and Arg-1 in the aortas of ApoE$^{-/-}$ mice (n=5) and RAW264.7 cells (n=5). (**D**) The BMDMs were evaluated following treatment with varying concentrations of QRHX, utilizing the Cell Counting Kit-8 assay (n=6). NC: normal diet; Model: high-fat diet; QRHX-L: QRHX low-dose group (HFD + 7.5 g/kg/d QRHX); QRHX-M: QRHX medium-dose group (HFD + 15 g/kg/d QRHX); QRHX-H: QRHX high-dose group (HFD + 30 g/kg/d QRHX). RAW: RAW264.7 cells; QRHX+RAW: RAW264.7 cells, QRHX intervention; BMDM-exo: RAW264.7 cells, BMDM-exo intervention; BMDM-QRHX-exo+RAW: RAW264.7 cells, BMDM-exo and QRHX intervention; BMDM-QRHX-exo +RAW+GW4869: RAW264.7 cells, BMDM-exo, QRHX, and GW4869 intervention. Data were presented as mean ± standard deviation (x ± s) in one-way ANOVA. *p<0.05, **p<0.01 vs NC group; $^{\#}$p<0.05, $^{\#}$p<0.01 vs MOD group. *p<0.05, **p<0.01 vs RAW group; $^{\#}$p<0.05, $^{\#\#}$p<0.01 vs BMDM-exo group.

QRHX Effect Was Elicited via the miR-26a-5p/PTGS2/NF-κB Signaling Pathway

We used Western blot to assess the expression of NF-κB signaling pathway components in vascular plaques of ApoE$^{-/-}$ mice as well as in RAW264.7 cells. In the in vivo experiments, Western blot analyses suggested that p65 and p50 was elevated in the MOD group, whereas the QRHX-M and QRHX-H groups showed decreased p65, and p50 protein expression (Figure 4A and B). RT-qPCR results showed that PTGS2 expression was increased in the MOD group compared with the NC group, and miR-26a-5p gene expression was decreased. Compared with the MOD group, PTGS2 gene expression was decreased and miR-26a-5p gene expressions were increased in the QRHXgroups (Figure 3E). In in vitro experiments, RAW264.7 cells, co-cultured with BMDM, showed decreased p65, p50 protein expression (Figure 3C and D), decreased PTGS2 gene expression, and elevated miR-26a-5p gene expression (Figure 3F). These effects were further enhanced by co-culture of BMDM with RAW264.7 after QRHX intervention (Figure 3C and D, F).

The above results suggest that QRHX can attenuate HFD-induced atherosclerotic inflammation through exosomal miR-26a-5p via inhibiting the PTGS2/NF-κB pathway on regulating macrophage polarization. To further validate these results, we transfected BMDMs using miR-26a-5p mimic and inhibitor lentivirus, and RAW264.7 cells using miR-26a-5p mimic and PTGS2 inhibitor lentivirus.

https://doi.org/10.2147/DDDT.S487476

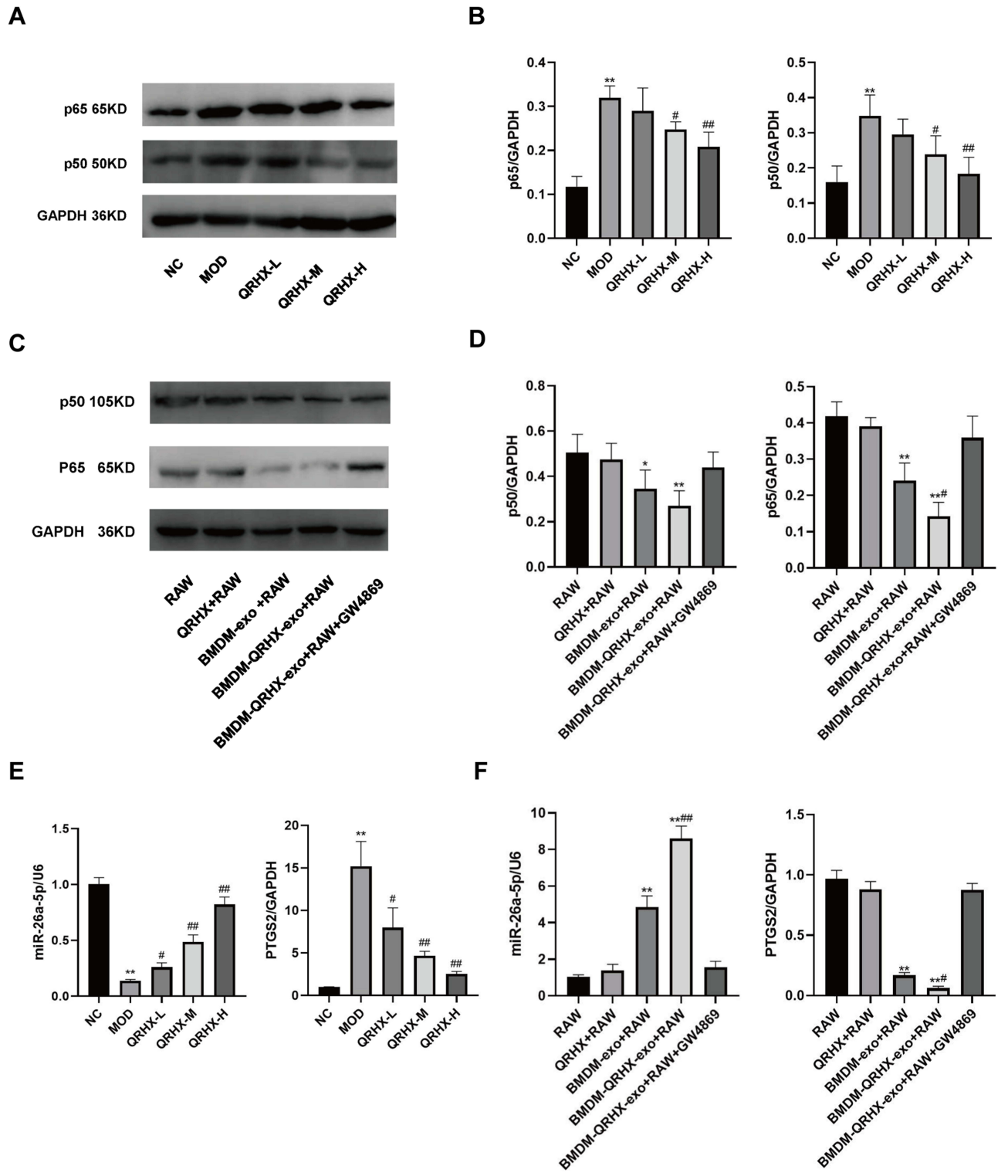

Figure 4 Effect of QRHX on miR-26a-5p/PTGS2/NF-κB signaling pathway in ApoE$^{-/-}$ mice and miR-26a-5p of BMDM-derived exosomes in RAW264.7. (**A**–**D**) Western blot analysis was conducted to assess the expression levels of p65 and p50 proteins in the aortas of ApoE$^{-/-}$ mice and RAW264.7 cells across each group (n=5). (**E** and **F**) RT-qPCR was employed to evaluate the expression levels of miR-26a-5p and PTGS2 genes in the aortas of ApoE$^{-/-}$ mice and RAW264.7 cells within each group. NC: normal diet, Model: high-fat diet, QRHX-L: QRHX low-dose group (HFD + 7.5 g/kg/d QRHX), QRHX-M: QRHX medium-dose group (HFD + 15 g/kg/d QRHX), QRHX-H: QRHX high-dose group (HFD + 30 g/kg/d QRHX). RAW: RAW264.7 cells; QRHX+RAW: RAW264.7 cells, QRHX intervention; BMDM-exo: RAW264.7 cells, BMDM-exo intervention; BMDM-QRHX-exo+RAW: RAW264.7 cells, BMDM-exo and QRHX intervention; BMDM-QRHX-exo+RAW+GW4869: RAW264.7 cells, BMDM-exo, QRHX, and GW4869 intervention. Data were presented as mean ± standard deviation (x ± s) in one-way ANOVA. *p<0.05, **p<0.01 vs NC group; $^{\#}$p<0.05, $^{\#}$p<0.01 vs MOD group. *p<0.05, **p<0.01 vs RAW group; $^{\#}$p<0.05, $^{\#\#}$p<0.01 vs BMDM-exo group.

The miR-26a-5p Regulated Macrophage Polarization by Targeting PTGS2 to Inhibit the NF-κB Pathway

First, we used a dual luciferase reporter assay to detect miR-26a-5p binding sites in the PTGS2 3 ‘-untranslated region (3 ‘utr). We cloned the PTGS2 wild-type 3 ‘utr or mutant 3 ‘utr of its putative miR-26a-5p binding site onto their corresponding plasmids and assessed their responsiveness to miR-26a-5p in 293T cells (Figure 5A). The results showed that miR-26a-5p directly bound the 3’-UTR of PTGS2 mRNA, and PTGS2 was a direct target of miR-26a-5p (Figure 5B). Secondly, we found that in co-culture, after overexpressing the miR-26a-5p level of BMDM, the iNOS gene expression, p65 and p50 protein expression of RAW264.7 was decreased, and Arg-1 gene expression was increased (Figure 5C and D, G). After inhibiting miR-26a-5p levels in BMDMs, iNOS gene expression, p65, and p50 protein expression were increased and Arg-1 gene expression was decreased in RAW264.7 (Figure 5C and D, 5G). In addition, after we directly overexpressed miR-26a-5p and inhibited PTGS2 on RAW264.7, respectively, the results showed that iNOS gene expression, p65, and p50 protein expression were decreased and Arg-1 gene expression was increased (Figure 5E and F, H). These results further suggested the possible role and relationship of miR-26a-5p and PTGS2 in macrophages. The miR-26a-5p of BMDM-exo exerts an effects by targeting PTGS2 in macrophages to suppress the NF-κB pathway to regulate M2 polarization.

BMDM-QRHX-Exo Attenuated Atherosclerosis in ApoE$^{-/-}$ Mice

We injected BMDM-derived exosomes (BMDM-exo) as well as QRHX-intervened exosomes (BMDM-QRHX-exo) back into ApoE$^{-/-}$ mice. There was no difference in the body weight of mice between the CON, BMDM-exo, and BMDM-QRHX-exo groups at eight weeks. Following an eight-week intervention, the body weights of mice in both the BMDM-exo and BMDM-QRHX-exo groups were lower than those in the CON group (Figure 6A). To validatethe anti-inflammatory properties of BMDM-QRHX-exo, ELISA was used to measure the levels of the inflammatory markers TNF-α and IL-10. Compared with the CON group, TNF-α levels were decreased and IL-10 levels were increased in both the BMDM-exo and BMDM-QRHX-exo groups of ApoE$^{-/-}$ mice, with the efficacy of the BMDM-QRHX-exo group being superior to that of the BMDM-exo group (Figure 6B). The results of oil red O staining on the entire aortic and H&E staining on the aortic root cross-section showed that the CON group had severe lipid deposition and large plaque areas. After exosome intervention, lipid deposition and plaque areas were reduced, with the effect being more pronounced after BMDM-QRHX-exo intervention (Figure 6C–F). The results of Masson staining showed that the BMDM-exo and BMDM-QRHX-exo groups reversed the decrease in collagen content compared with the CON group. Macrophages are important inflammatory cells in AS lesions, and we used MOMA-2 to assess the presence of macrophages in vascular plaques. Compared with the CON group, we observed different levels of macrophage reduction in the BMDM-exo and BMDM-QRHX-exo groups, with macrophage infiltration being the mildest in the BMDM-QRHX -exo group (Figure 6D and F), suggesting that BMDM-QRHX-exo can reduce macrophage infiltration and attenuate inflammatory responses.

BMDM-QRHX-Exo Regulated Macrophage Polarization via miR-26a-5p/PTGS2/NF-κB Signaling Pathway in ApoE$^{-/-}$ Mice

In vivo experiments of exosome reinjection showed that iNOS, TNF-α, p65, and p50 protein expression was decreased, while Arg-1, Ym-1, and Fizz-1 protein expression was elevated in the BMDM-exo and BMDM-QRHX-exo groups compared to the CON group (Figure 7A–E). RT-qPCR indicated that PTGS2, iNOS gene expression was decreased and Arg-1, miR-26a-5p gene expression was increased in the BMDM-exo and BMDM-QRHX-exo groups compared to the CON group (Figure 7F). The BMDM-QRHX-exo groups had decreased PTGS2, TNF-α and p65 expression and increased Arg-1 and miR-26a-5p gene expression compared to the BMDM-exo group (Figure 7F). These results suggest that QRHX could improve AS by upregulating miR-26a-5p, downregulating PTGS2, inhibiting the NF-κB pathway, and regulating macrophage polarization from M1 to M2 via exosomal miR-26a-5p.

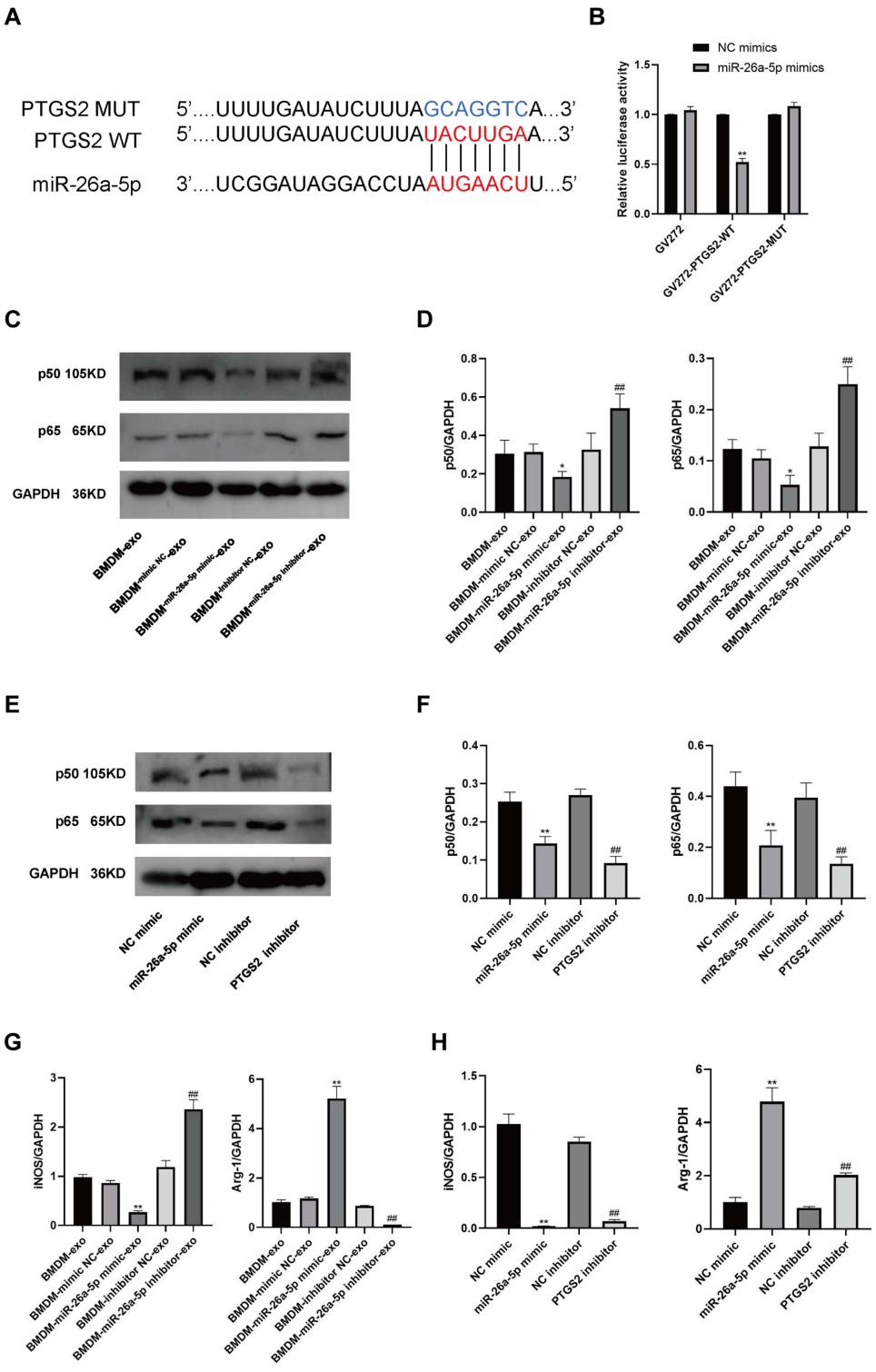

Figure 5 PTGS2 is a target gene of miR-26a-5p. miR-26a-5p regulation of PTGS2 affects the NF-κB signaling pathway and macrophage polarization. (**A**) The binding site prediction maps for miR-26a-5p and both wild-type (WT) and mutant (MUT) PTGS2 are presented. (**B**) Results from the dual luciferase reporter assay are shown (n=6). (**C**–**F**) Western blot analyses were conducted to assess the protein expression levels of p65 and p50 in RAW264.7 cells (n=5). (**G** and **H**) RT-qPCR was performed to measure the expression levels of the iNOS and Arg-1 genes in RAW264.7 cells. BMDM-exo: RAW264.7 cells, BMDM-exo; BMDM-mimic NC-exo: RAW264.7 cells, BMDM-exo (mimic vector); BMDM-miR-26a-5p mimic-exo: RAW264.7 cells, BMDM-exo (miR-26a-5p mimic); BMDM-inhibitor NC-exo: RAW264.7 cells, BMDM-exo (inhibitor vector); BMDM-miR-26a-5p inhibitor-exo: RAW264.7 cells, BMDM-exo (miR-26a-5p inhibitor). NC mimic: RAW264.7 cells (mimic vector); miR-26a-5p mimic: RAW264.7 cells (miR-26a-5p mimic); NC inhibitor: RAW264.7 cells (inhibitor vector); PTGS2 inhibitor: RAW264.7 cells (PTGS2 inhibitor). Data were presented as mean ± standard deviation (x ± s) in one-way ANOVA. *p<0.05, **p<0.01 vs NC mimics group. *p<0.05, **p<0.01 vs BMDM-mimic NC-exo group; #p<0.05, ##p<0.01 vs BMDM-inhibitor NC-exo group. *p<0.05, **p<0.01 vs NC mimic group; #p<0.05, ##p<0.01 vs NC inhibitor group.

 https://doi.org/10.2147/DDDT.S487476

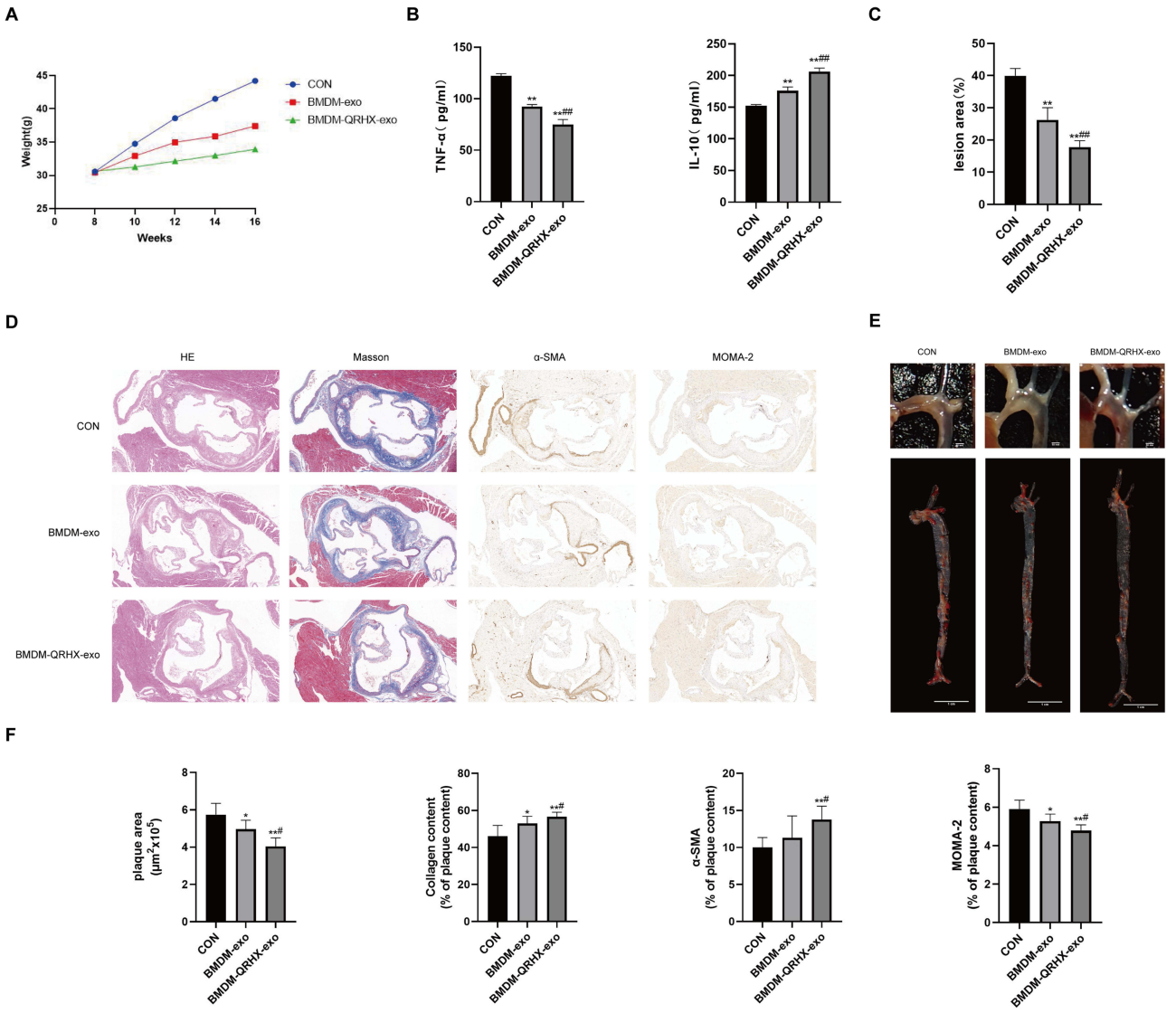

Figure 6 QRHX and miR-26a-5p of BMDM-derived exosomes attenuate atherosclerosis in HFD-fed ApoE$^{-/-}$ mice. (**A**) Body weight of ApoE$^{-/-}$ mice (n=10). 0~8 weeks: HFD induction; 9~16 weeks: HFD induction, QRHX intervention. (**B** and **D**) H&E, Masson, α-SMA, MOMA-2 staining. For Masson, α-SMA, and MOMA-2 staining, the ratio is the relative area of the stained area within the plaque to the total area of the plaque (n=5). Scale bar: 100 μm. (**C** and **F**) The oil red O staining on the entire aorta of ApoE$^{-/-}$ mice. The ratio is the relative area of stained area for lipid deposits to the relative area of total aortic area (n=5). (**E**) ELISA for serum levels of TNF-α and IL-10 (n=10). CON: high-fat diet, 200 μL PBS injected in the tail vein; BMDM-exo: high-fat diet, BMDM-derived exosomes (10^{10}/each, dissolution in 200 μL PBS injected in the tail vein); BMDM-QRHX-exo: high-fat diet, BMDM-derived exosomes of QRHX intervention (10^{10}/each, dissolution in 200 μL PBS injected in the tail vein). Data were presented as mean ± standard deviation (x ± s) in one-way ANOVA. *p<0.05, **p<0.01 vs CON group; #p<0.05, ##p<0.01 vs BMDM-exo group.

Discussion

In the study, we found that BMDM-exo attenuates inflammation and AS. Second, we found that miR-26a-5p in BMDM-exo could promote macrophage polarization via inhibiting the PTGS2/NF-κB signaling pathway. Finally, we verified that QRHX can improve AS by regulating macrophage polarization through exosomal miR-26a-5p via inhibiting the PTGS2/NF-κB pathway.

The incidence of AS is increasing rapidly, driven by societal aging and improved living conditions.[61] AS can affect major arteries, including the coronary, aortic, and cerebral arteries. As AS advances, there is a marked decrease in plaque stability, which predisposes individuals to high-risk events such as acute coronary syndromes and stroke, along with other complications.[62] Statins are commonly prescribed as first-line medications for the prevention and treatment of AS. However, some individuals exhibit poor responses to statins, and some patients with severe dyslipidemia find that statins are ineffective when used alone.[63,64] TCM has been attracted more attention in the treatment of AS due to its safety and

https://doi.org/10.2147/DDDT.S487476

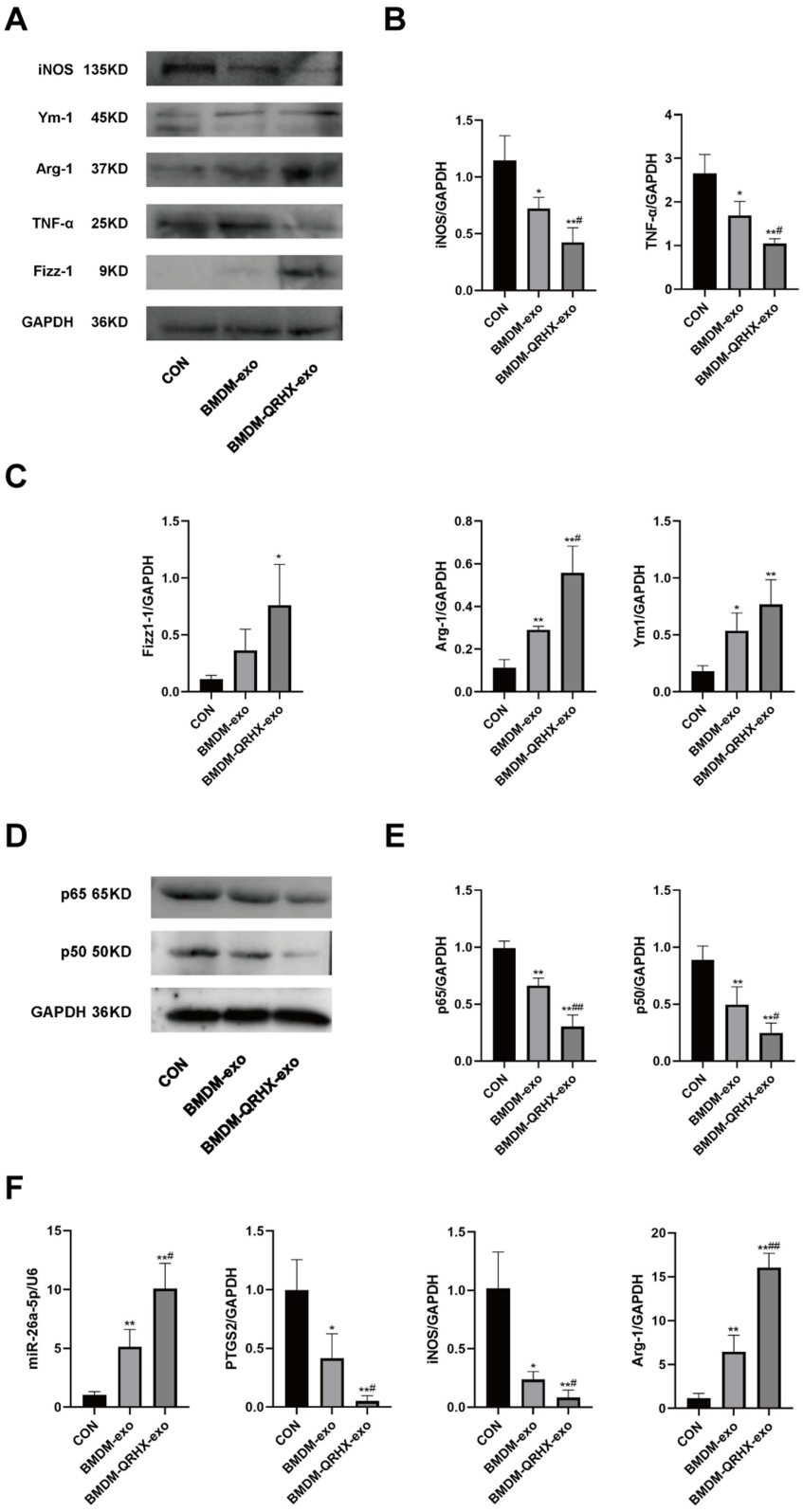

Figure 7 Effects of QRHX and miR-26a-5p of BMDM-derived exosomes on miR-26a-5p/PTGS2/NF-κB signaling pathway and macrophage polarization in ApoE$^{-/-}$ mice. (**A**–**E**) Western blot to detect the protein expression of iNOS, TNF-α, Arg-1, Ym-1, Fizz-1, p65, and p50 in aortas of ApoE$^{-/-}$ mice in each group (n=5). (**F**) RT-qPCR was performed to detect miR-26a-5p, PTGS2, iNOS, and Arg-1 gene expression levels in the aorta of ApoE$^{-/-}$ mice in each group. CON: high-fat diet, 200 μL PBS injected in the tail vein; BMDM-exo: high-fat diet, BMDM-derived exosomes (10^{10}/each, dissolution in 200 μL PBS injected in the tail vein); BMDM-QRHX-exo: high-fat diet, BMDM-derived exosomes of QRHX intervention (10^{10}/each, dissolution in 200 μL PBS injected in the tail vein). Data were presented as mean ± standard deviation (x ± s) in one-way ANOVA. *p<0.05, **p<0.01 vs CON group; #p<0.05, ##p<0.01 vs BMDM-exo group.

efficacy.[65–67] TCM has the potential to mitigate certain symptoms and overcome some limitations associated with conventional pharmacological treatments.[68,69] QRHX has been used in the prevention and treatment of AS for 20 years and achieved well curative effect.[22–24] Our findings elucidate the fundamental molecular mechanisms underlying the QRHX intervention in AS, potentially related to the delivery of exosomes. However, the current technical challenges associated with the mass production and purification of exosomes necessitate further research. As the study progresses, our results may provide evidence for clinical.

The more popular method for creating an animal model of AS in the research is to choose $ApoE^{-/-}$ mice that are fed an HFD.[70] During the current experimental study, no physiological manifestations indicative of toxic response,[57,71] such as mortality, fatigue, unresponsiveness, or altered gait, were observed in mice. Our study indicated that the MOD group had higher plaque area and lipid deposition compared to the NC group, suggesting that $ApoE^{-/-}$ mice were an effective model for AS. When the dose of QRHX was raised, compared to the MOD group, the plaques in the aorta gradually decreased and the SMCs increased. This suggests that QRHX can alleviate AS and has a plaque-stabilizing impact in the $ApoE^{-/-}$ mice.

Oxidized low-density lipoprotein (ox-LDL) is consumed by monocyte-derived macrophages, which then produce cytokines that promote inflammation. Macrophage polarization, proliferation, and even cell death are triggered by dendritic cells and mast cells, as well as by cytokines and histamine produced beyond lipid accumulation.[72,73] Numerous pro-inflammatory factors have been identified as contributing to the development and progression of AS, with TNF-α being one of the representative pro-inflammatory factors.[74,75] Furthermore, anti-inflammatory factors exist, with IL-10 being a common anti-inflammatory cytokine.[76] The expression of IL-10 is critical for the prevention of AS.[77] It was found that, in comparison to the MOD group, both the QRHX-M and QRHX-H groups exhibited a reduction in TNF-α levels and alongside a increase in IL-10 levels. These findings support the ability of anti-inflammatory properties of QRHX.

In AS, macrophage polarization induces atherosclerotic plaque instability and accelerates AS progression.[78] Modulation of macrophage responses to lipids and other pro-inflammatory compounds may be a promising target for AS therapies.[79] TCM and herbal extracts can regulate macrophage polarization to improve AS. Yang-Xin-Shu-Mai granule may alleviate AS by suppressing the TLR9/MyD88/NF-κB pathway.[80] Additionally, it appears to reprogram macrophage polarization from the M1 to M2 phenotype, thereby reducing vascular inflammation.[80] Curcumin may improve AS through potential effects on cell migration, proliferation, cholesterol homeostasis, and inflammation,[81] and also modulates macrophage polarization, potentially through the TLR4/MAPK/NF-κB pathway.[82] In our study, we observed that QRHX treatment led to a reduction in the expression of the M1 macrophage marker iNOS, while concurrently increasing the expression of the M2 macrophage marker Arg-1. These findings suggest that QRHX may promote a shift in macrophage polarization towards an anti-inflammatory M2 phenotype in HFD-induced AS mice, which could be beneficial in mitigating the inflammatory processes associated with AS. The NF-κB signaling pathway plays a crucial role in the regulation of immune cell activation, maturation, and polarization.[83] Inhibition of this pathway facilitates the polarization of macrophages from the M1 to the M2 phenotype, thereby reducing inflammatory damage.[84–86] To understand how QRHX regulates macrophage polarization, we examined the NF-κB pathway.

The widely distributed transcription factor NF-κB plays an important role in immunological response, inflammatory response, cytoplasmic/nuclear signaling, and developmental processes. However, this pathway is sensitive to a variety of stimuli.[87] Moreover, the NF-κB pathway is a critical target for interventions aimed at modulating macrophage polarization in AS.[88–90] By targeting this pathway, it is possible to influence the balance between pro-inflammatory M1 and anti-inflammatory M2 macrophages, thereby potentially reducing inflammation and slowing the progression of AS. When the NF-κB signaling pathway receives a stimulus, the macrophage polarization phenotype may be altered as well.[91] As expected, our study revealed that QRHX intervention resulted in suppressing the NF-κB pathway and regulating macrophage polarization from M1 to M2. These findings indicate that QRHX may regulate macrophage polarization via the NF-κB pathway.

Cyclooxygenase-2 (COX-2), also known as PTGS2, is an enzyme involved in the production of prostaglandins, which are important inflammatory mediators in the human body. The pathophysiology of AS is exacerbated and caused by the activation of the COX-2 signaling pathway.[92] Research has demonstrated that a range of inflammatory cytokines affect

the expression of COX-2, which is found in atherosclerotic lesions.[93] Metabolites of COX-2 are known to promote inflammatory responses, suggesting that COX-2 plays a pivotal role in the pathological process and progression of AS.[94,95] Owing to the significance of COX-2 in inflammation, elevated COX-2 expression in tissues has emerged as a crucial indicator of inflammation.[96] In our study, we found that miR-26a-5p is decreased and PTGS2 is increased in HFD-fed ApoE$^{-/-}$ mice and that miR-26a-5p and PTGS2 levels are improved after QRHX intervention. The same results were also observed in vitro experiments. Our study also found that after inhibition of PTGS2, the NF-κB pathway was suppressed and macrophages were polarized from M1 to M2, suggesting that PTGS2 may inhibit the NF-κB pathway and regulate macrophage polarization.

Almost all types of cells release exosomes, and miRNAs are key carriers for exosome function.[97] It is worth noting that numerous studies have demonstrated that exosomal miRNAs are closely related to AS. For instance, exosomes released by sleep deprivation exacerbate AS by decreasing miR-182-5p, which upregulates MYD88 and activates the NF-κB/NLRP3 pro-inflammatory pathway.[98] The obesity-induced exosome miR-27b-3p enters vascular endothelial cells and promotes inflammation and AS by inhibiting PPARα/NF-κB.[99] Meanwhile, some researchers have suggested that exosomes produced from BMDMs, mesenchymal stem cells, and endothelial progenitor cells (EPCs) have been reported to improve AS.[100] A growing body of studies have demonstrated that miRNAs play a critical role in macrophage polarization. By targeting NF-κB and TNF-α signaling pathways, miRNAs of BMDM-derived exosomes suppress inflammation and promote M2 polarization in recipient macrophages.[9] Among miRNAs, miR-26a-5p is involved in many cellular biological processes and exhibits diverse biological functions. The miR-26a is abnormally expressed in various cardiovascular diseases, such as myocardial ischemia,[101] myocardial hypertrophy,[102] and AS.[103] A recent study showed that overexpressing miR-26a enhances cell viability and inhibits the NF-κB pathway, inflammation, and apoptosis. The miR-26a plays a role in cell differentiation, proliferation, apoptosis, and metastasis. These findings imply that miR-26a-5p may be crucial in slowing the advancement of AS. In our study, we found that exosomes derived from C57BL/6J mice-derived BMDMs expressed higher levels of miR-26a-5p compared to those derived from ApoE$^{-/-}$ mice. Dual luciferase reporter assay confirmed that miR-26a-5p directly binds to the 3'-UTR of PTGS2 mRNA, indicating that PTGS2 is a direct target of miR-26a-5p. We injected BMDM-exo back into ApoE$^{-/-}$ mice via the tail vein and confirmed that BMDM-exo carrying miR-26a-5p ameliorated AS. Concurrently, BMDM-exo increased miR-26a-5p levels and decreased PTGS2 levels and inhibited the NF-κB signaling pathway, and polarized macrophage from M1 to M2 in ApoE$^{-/-}$ mice. Additionally, we demonstrated that QRHX could intervene in AS through exosomal miR-26a-5p and elucidating a novel mechanism of QRHX intervention in AS.

There have been many previous studies on the treatment of AS with TCM compound,[104,105] but there are almost no studies on the mechanism of TCM compound in the treatment of AS through exosomal miRNAs. Recent studies have indicated the role of exosomes in facilitating intercellular communication, as well as their potential as diagnostic and therapeutic tools for a range of diseases, including AS.[106,107] Our study investigated how QRHX modulates exosomal miR-26a-5p to ameliorate AS, both showing the benefits of QRHX and addressing the underlying molecular processes involved in QRHX intervention in AS.

While it was demonstrated that QRHX has a regulatory effect on macrophages via exosomal miR-26a-5p on the PTGS2/NF-κB pathways, the current study is not without limitations. Firstly, the improvement of targeting of exosomes when they are used as drug carriers is associated with the modification of the surface glycoconjugates.[108] We have investigated the relationship between QRHX and exosomes, and need further investigate the targeting of drug delivery by modifying the glycoconjugates on the exosomes. This could improve the specificity of QRHX intervention on exosomal drug delivery. Secondly, as research progressed, macrophage phenotypes were further delineated, such as M2a, M2b, M2c. We have conducted a preliminary examination of the impact of QRHX on the M1 to M2 phenotypic transition of macrophages within AS plaques, an in-depth analysis of specific macrophage subtypes remains to be conducted. The potential differences in the regulation of miR-26a-5p expression by QRHX across various macrophage subtypes remain uncertain. Furthermore, due to limitations in time and financial resources, macrophage-specific knockout mice were not utilized for additional in vivo experiments. Finally, AS is a chronic condition. Due to financial and time constraints, we were unable to establish a longer-term experimental model for observation. Therefore, further research is needed to investigate the long-term anti-inflammatory and anti-AS effects of QRHX.

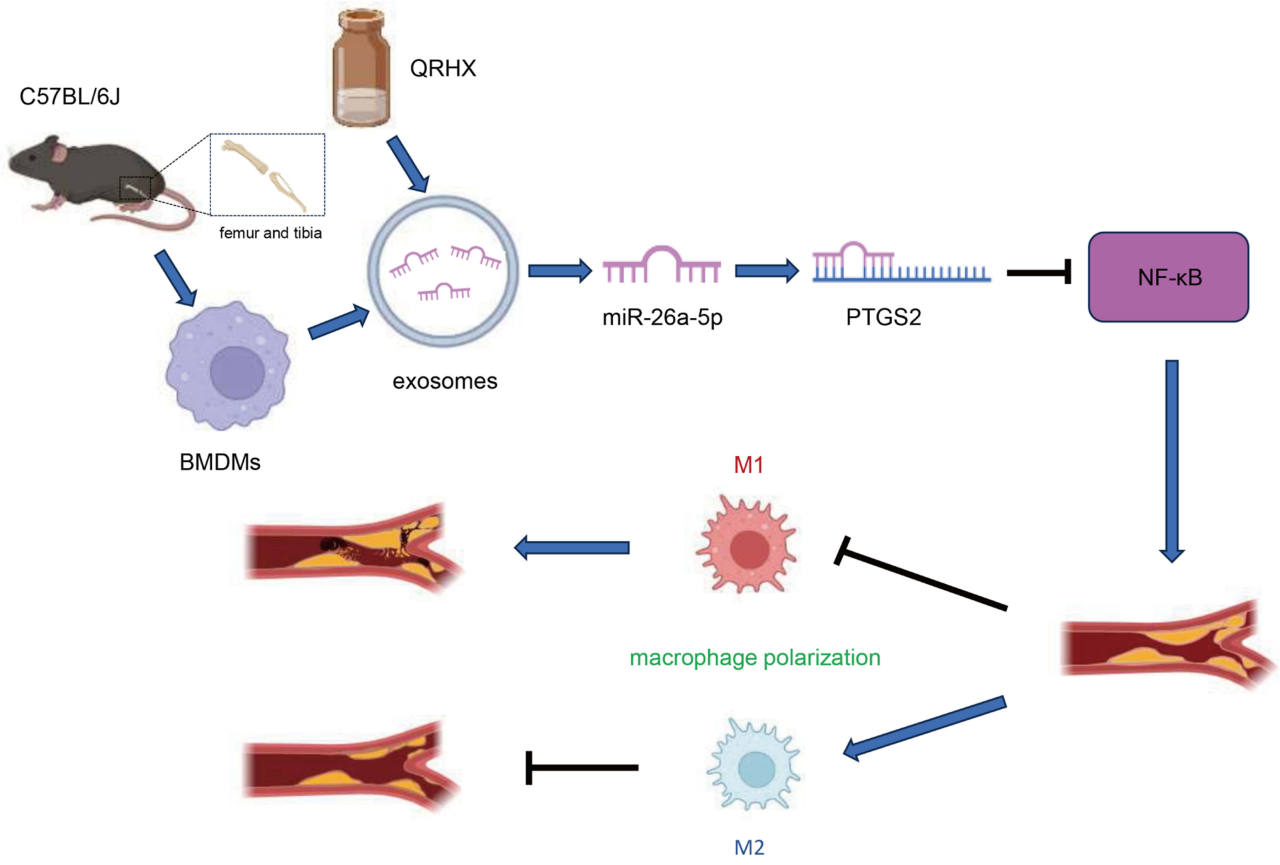

Figure 8 Graphical mechanism by which QRHX and miR-26a-5p of BMDM-derived exosomes attenuate HFD-induce atherosclerosis. QRHX can play an anti-inflammatory and plaque-stabilizing role by mediating the exosomal miR-26a-5p via inhibiting PTGS2/NF-κB signaling pathway and regulating the macrophage phenotype in AS plaques from M1 to M2 polarization.

Conclusion

This study evaluated the relationship between QRHX, exosomal miR-26a-5p, and AS. Our findings indicate that QRHX inhibits the PTGS2/NF-κB signaling pathway, subsequently modulating the macrophage phenotype within AS plaques from M1 to M2 polarization. The effects were more pronounced with a higher dose of QRHX compared to the middle and low doses. This modulation enables QRHX to exert plaque-stabilizing effects via exosomal miR-26a-5p (Figure 8). These results elucidate the underlying mechanisms linking QRHX, exosomal miR-26a-5p, and AS, offering a novel perspective for TCM intervention in AS and broadening the scope of the TCM approach of clearing heat and activating blood.

Abbreviations

AS, atherosclerosis; HFD, high-fat diet; ASCVD, arteriosclerotic cardiovascular disease; NF-κB, nuclear factor kappa-B; PTGS2, prostaglandin-endoperoxide synthase 2; BMDM, Bone marrow-derived macrophages; H&E, hematoxylin-eosin; α-SMA, α-smooth muscle actin; SMC, smooth muscle cells; MOMA-2, Monocyte + Macrophage; Ox-LDL, oxidized low-density lipoprotein; EVs, Extracellular vesicles; iNOS, inducible nitric oxide synthase; Arg-1, Arginase-1; Fizz-1, resistin-like-α; YM-1, chitinase 3-like 3; p65, nuclear factor kappa B(NF-κB)65 kDa polypeptide; LDL-C, low-density lipoprotein cholesterol; PCSK9, Proprotein convertase subtilisin/kexin type 9; TCM, Traditional Chinese Medicine; UPLC-MS, ultra-performance liquid chromatography-mass spectrometry; NSTEMI, non-ST-segment elevation myocardial infarction; STEMI, ST-segment elevation myocardial infarction; PCI, percutaneous coronary intervention; TLR9, Toll-like receptor 9; MyD88, myeloid differentiation primary response 88; ELISA, Enzyme-Linked Immunosorbent Assay; TNF -α, Tumor necrosis factor -α; IL-10, Interleukin-10; IL-1β, interleukin 1β; IL-17, interleukin 17; OD, optical

https://doi.org/10.2147/DDDT.S487476

density; CD63,Cluster of Differentiation 63; TSG101, tumor susceptibility 101; CCK8, Cell Counting Kit-8; ApoE-/-, Apolipoprotein E knockout; PGE2, Prostaglandin E2; RT-qPCR, Realtime fluorescence quantitative PCR; ox-LDL, Oxidized low-density lipoprotein; COX-2, cyclooxygenase-2.

Data Sharing Statement

Data will be made available on request and can be obtained from the corresponding author.

Author Contributions

All authors made a significant contribution to the work reported, whether that is in the conception, study design, execution, acquisition of data, analysis and interpretation, or in all these areas; took part in drafting, revising or critically reviewing the article; gave final approval of the version to be published; have agreed on the journal to which the article has been submitted; and agree to be accountable for all aspects of the work.

Funding

This study was supported by grants from the National Natural Science Foundation of China (82204984, 82204987) and the Youth Project of Guangdong Natural Science Foundation (No. 2021A1515110287).

Disclosure

The author reports no conflicts of interest in this work.

References

1. Hiwasa T, Zhang XM, Kimura R, et al. Elevated adiponectin antibody levels in sera of patients with atherosclerosis-related coronary artery disease, cerebral infarction and diabetes mellitus. *J Circ Biomark*. 2016;5:8. doi:10.5772/63218
2. Hou P, Fang J, Liu Z, et al. Macrophage polarization and metabolism in atherosclerosis. *Cell Death Dis*. 2023;14(10):691. doi:10.1038/s41419-023-06206-z
3. Stoger JL, Gijbels MJ, van der Velden S, et al. Distribution of macrophage polarization markers in human atherosclerosis. *Atherosclerosis*. 2012;225(2):461–468. doi:10.1016/j.atherosclerosis.2012.09.013
4. Otsuka F, Sakakura K, Yahagi K, Joner M, Virmani R. Has our understanding of calcification in human coronary atherosclerosis progressed? *Arterioscler Thromb Vasc Biol*. 2014;34(4):724–736. doi:10.1161/ATVBAHA.113.302642
5. Davis FM, Gallagher KA. Epigenetic mechanisms in monocytes/macrophages regulate inflammation in cardiometabolic and vascular disease. *Arterioscler Thromb Vasc Biol*. 2019;39(4):623–634. doi:10.1161/ATVBAHA.118.312135
6. Liu Y, Wang X, Pang J, et al. Attenuation of atherosclerosis by protocatechuic acid via inhibition of M1 and promotion of M2 macrophage polarization. *J Agric Food Chem*. 2019;67(3):807–818. doi:10.1021/acs.jafc.8b05719
7. Xin D, Li T, Chu X, et al. Mesenchymal stromal cell-derived extracellular vesicles modulate microglia/macrophage polarization and protect the brain against hypoxia-ischemic injury in neonatal mice by targeting delivery of miR-21a-5p. *Acta Biomater*. 2020;113:597–613. doi:10.1016/j.actbio.2020.06.037
8. Hayden MS, Ghosh S. Regulation of NF-kappaB by TNF family cytokines. *Semin Immunol*. 2014;26(3):253–266. doi:10.1016/j.smim.2014.05.004
9. Bouchareychas L, Duong P, Covarrubias S, et al. Macrophage exosomes resolve atherosclerosis by regulating hematopoiesis and inflammation via MicroRNA cargo. *Cell Rep*. 2020;32(2):107881. doi:10.1016/j.celrep.2020.107881
10. Han C, Yang J, Sun J, Qin G. Extracellular vesicles in cardiovascular disease: biological functions and therapeutic implications. *Pharmacol Ther*. 2022;233:108025. doi:10.1016/j.pharmthera.2021.108025
11. Wu R, Gao W, Yao K, Ge J. Roles of exosomes derived from immune cells in cardiovascular diseases. *Front Immunol*. 2019;10:648. doi:10.3389/fimmu.2019.00648
12. Ward NC, Watts GF, Eckel RH. Statin Toxicity. *Circ Res*. 2019;124(2):328–350. doi:10.1161/CIRCRESAHA.118.312782
13. Cannon CP, Blazing MA, Giugliano RP, et al. Ezetimibe added to statin therapy after acute coronary syndromes. *N Engl J Med*. 2015;372(25):2387–2397. doi:10.1056/NEJMoa1410489
14. Kim BK, Hong SJ, Lee YJ, et al. Long-term efficacy and safety of moderate-intensity statin with ezetimibe combination therapy versus high-intensity statin monotherapy in patients with atherosclerotic cardiovascular disease (RACING): a randomised, open-label, non-inferiority trial. *Lancet*. 2022;400(10349):380–390. doi:10.1016/S0140-6736(22)00916-3
15. O'Donoghue ML, Fazio S, Giugliano RP, et al. Lipoprotein(a), PCSK9 inhibition, and cardiovascular risk. *Circulation*. 2019;139(12):1483–1492. doi:10.1161/CIRCULATIONAHA.118.037184
16. Schwartz GG, Steg PG, Szarek M, et al. Alirocumab and cardiovascular outcomes after acute coronary syndrome. *N Engl J Med*. 2018;379(22):2097–2107. doi:10.1056/NEJMoa1801174
17. Li JJ, Lu ZL, Kou WR, et al. Impact of Xuezhikang on coronary events in hypertensive patients with previous myocardial infarction from the china coronary secondary prevention study (CCSPS). *Ann Med*. 2010;42(3):231–240. doi:10.3109/07853891003652534

18. Venero CV, Venero JV, Wortham DC, Thompson PD. Lipid-lowering efficacy of red yeast rice in a population intolerant to statins. *Am J Cardiol*. 2010;105(5):664–666. doi:10.1016/j.amjcard.2009.10.045
19. Shi Y, Liu C, Xiong S, et al. Ling-Gui-Qi-Hua formula alleviates left ventricular myocardial fibrosis in rats with heart failure with preserved ejection fraction by blocking the transforming growth factor-beta1 /Smads signaling pathway. *J Ethnopharmacol*. 2023;317:116849. doi:10.1016/j.jep.2023.116849
20. Guo H, Li P, Zhao J, et al. Sheng Mai Yin shows anti-fatigue, anti-hypoxia and cardioprotective potential in an experimental joint model of fatigue and acute myocardial infarction. *J Ethnopharmacol*. 2024;319(Pt 3):117338. doi:10.1016/j.jep.2023.117338
21. Duan S, Zhang M, Zeng H, et al. Integrated proteomics and phosphoproteomics profiling reveals the cardioprotective mechanism of bioactive compounds derived from Salvia miltiorrhiza Burge. *Phytomedicine*. 2023;117:154897. doi:10.1016/j.phymed.2023.154897
22. Zuo Q, Chu Q, Jin Z, et al. Qingre huoxue decoction for treatment of acute st segment elevation myocardial infarction: a prospective multicenter cohort study[in Chinese]. *J Tradit Chin Med*. 2021;62(3):229–234.
23. Wu W, Peng R, Li R, et al. Effect of qingre huoxue decoction on the 60 coronary heart disease patients with acute myocardial Infarction[in Chinese]. *J Tradit Chin Med*. 2012;51(10):905–908.
24. Jin Z, Luo Y, Zhao H, et al. Qingre huoxue decoction regulates macrophage polarisation to attenuate atherosclerosis through the inhibition of NF-kappaB signalling-mediated inflammation. *J Ethnopharmacol*. 2023;301:115787. doi:10.1016/j.jep.2022.115787
25. World Health Organization. *WHO International Standard Terminologies on Traditional Chinese Medicine*. Geneva: World Health Organization; 2022. Licence: CC BY-NC-SA 3.0 IGO.
26. Lu X. Introduction to Ding Shuwen's experience in treating coronary heart disease from the heat-toxicity theory. *J Emergency Traditional Chin Med*. 2011;20(10):1597–1607.
27. Wu W, Peng R. Exploration of the pathogenesis of heat toxin in coronary heart disease[in Chinese]. *J New Chin Med*. 2007;2007(6):3–4.
28. Chen C, Lei L. Exploration of the correlation between inflammatory mechanism and heat toxin, phlegm and stasis in coronary heart disease. *J Emergency Traditional Chin Med*. 2007;2007(03):311–312.
29. Chu Q, Tang N, Lu J, et al. Effect of qingre huoxue decoction on TCM syndrome curative effect and relationship with macrophage polarization phenotype M2[in Chinese]. *J. Liaoning Univ of TCM*. 2020;22(4):158–162.
30. Commission of chinese pharmacopoeia. *Chin Pharmacopoeia*. 2020;2020.
31. Liu W, Deng B, Li R, Al E. Qingre huoxue decoctione make the intervention effect on patients who suffer the renal damage from contrast agent after percutaneous coronary intervention operation[in Chinese]. *J. Liaoning Univ of TCM*. 2015;17(6):184–187.
32. Jin Z, Zhang W, Luo Y, et al. Protective effect of qingre huoxue decoction against myocardial infarction via PI3K/Akt autophagy pathway based on UPLC-MS, network pharmacology, and in vivo evidence. *Pharm Biol*. 2021;59(1):1607–1618. doi:10.1080/13880209.2021.2001542
33. Dinda B, Dinda S, DasSharma S, et al. Therapeutic potentials of baicalin and its aglycone, baicalein against inflammatory disorders. *Eur J Med Chem*. 2017;131:68–80. doi:10.1016/j.ejmech.2017.03.004
34. Duan L, Zhang Y, Yang Y, et al. Baicalin inhibits ferroptosis in intracerebral hemorrhage. *Front Pharmacol*. 2021;12:629379. doi:10.3389/fphar.2021.629379
35. Shahzadi I, Ali Z, Bukhari S, et al. Possible applications of salvianolic acid B against different cancers. *Explor Target Antitumor Ther*. 2020;1(4):218–238. doi:10.37349/etat.2020.00014
36. Li M, Lu Y, Hu Y, et al. Salvianolic acid B protects against acute ethanol-induced liver injury through SIRT1-mediated deacetylation of p53 in rats. *Toxicol Lett*. 2014;228(2):67–74. doi:10.1016/j.toxlet.2014.04.011
37. Wu Y, Wang F, Fan L, et al. Baicalin alleviates atherosclerosis by relieving oxidative stress and inflammatory responses via inactivating the NF-kappaB and p38 MAPK signaling pathways. *Biomed Pharmacother*. 2018;97:1673–1679. doi:10.1016/j.biopha.2017.12.024
38. Zhu W, Jin Z, Yu J, et al. Baicalin ameliorates experimental inflammatory bowel disease through polarization of macrophages to an M2 phenotype. *Int Immunopharmacol*. 2016;35:119–126. doi:10.1016/j.intimp.2016.03.030
39. Lai YS, Putra R, Aui SP, Chang KT. M2(C) polarization by baicalin enhances efferocytosis via upregulation of MERTK receptor. *Am J Chin Med*. 2018;46(8):1899–1914. doi:10.1142/S0192415X18500957
40. Zhao Y, Shao C, Zhou H, et al. Salvianolic acid B inhibits atherosclerosis and TNF-alpha-induced inflammation by regulating NF-kappaB/NLRP3 signaling pathway. *Phytomedicine*. 2023;119:155002. doi:10.1016/j.phymed.2023.155002
41. Zou T, Gao S, Yu Z, et al. Salvianolic acid B inhibits RAW264.7 cell polarization towards the M1 phenotype by inhibiting NF-kappaB and Akt/mTOR pathway activation. *Sci Rep*. 2022;12(1):13857. doi:10.1038/s41598-022-18246-0
42. Zhao M, Li F, Jian Y, et al. Salvianolic acid B regulates macrophage polarization in ischemic/reperfused hearts by inhibiting mTORC1-induced glycolysis. *Eur J Pharmacol*. 2020;871:172916. doi:10.1016/j.ejphar.2020.172916
43. Brand K, Page S, Rogler G, et al. Activated transcription factor nuclear factor-kappa B is present in the atherosclerotic lesion. *J Clin Invest*. 1996;97(7):1715–1722. doi:10.1172/JCI118598
44. Funes SC, Rios M, Escobar-Vera J, Kalergis AM. Implications of macrophage polarization in autoimmunity. *Immunology*. 2018;154(2):186–195. doi:10.1111/imm.12910
45. Yan G, Wang J, Fang Z, Yan S, Zhang Y. MiR-26a-5p targets WNT5A to protect cardiomyocytes from injury due to hypoxia/reoxygenation through the Wnt/beta-catenin signaling pathway. *Int Heart J*. 2021;62(5):1145–1152. doi:10.1536/ihj.21-054
46. Li J, Tong Y, Zhou Y, et al. LncRNA KCNQ1OT1 as a miR-26a-5p sponge regulates ATG12-mediated cardiomyocyte autophagy and aggravates myocardial infarction. *Int J Cardiol*. 2021;338:14–23. doi:10.1016/j.ijcard.2021.05.053
47. Xing X, Guo S, Zhang G, et al. miR-26a-5p protects against myocardial ischemia/reperfusion injury by regulating the PTEN/PI3K/AKT signaling pathway. *Braz J Med Biol Res*. 2020;53(2):e9106. doi:10.1590/1414-431x20199106
48. Lu Y, Liu M, Guo X, et al. miR-26a-5p alleviates CFA-induced chronic inflammatory hyperalgesia through Wnt5a/CaMKII/NFAT signaling in mice. *CNS Neurosci Ther*. 2023;29(5):1254–1271. doi:10.1111/cns.14099
49. Chen Y, Zhou X, Wu Y. The miR-26a-5p/IL-6 axis alleviates sepsis-induced acute kidney injury by inhibiting renal inflammation. *Ren Fail*. 2022;44(1):551–561. doi:10.1080/0886022X.2022.2056486
50. Bian J, Ge W, Jiang Z. miR-26a-5p attenuates oxidative stress and inflammation in diabetic retinopathy through the USP14/NF-kappaB signaling pathway. *J Ophthalmol*. 2024;2024:1470898. doi:10.1155/2024/1470898

51. Shi H, Li H, Zhang F, et al. MiR-26a-5p alleviates cardiac hypertrophy and dysfunction via targeting ADAM17. *Cell Biol Int*. 2021;45 (11):2357–2367. doi:10.1002/cbin.11685
52. Mompeon A, Perez-Cremades D, Paes AB, et al. Circulating miRNA fingerprint and endothelial function in myocardial infarction: comparison at acute event and one-year follow-up. *Cells*. 2022;11(11):1823. doi:10.3390/cells11111823
53. Yang X, Du X, Ma K, et al. Circulating miRNAs related to long-term adverse cardiovascular events in STEMI patients: a nested case-control study. *Can J Cardiol*. 2021;37(1):77–85. doi:10.1016/j.cjca.2020.03.018
54. Yin J, Zhao X, Chen X, Shen G. Emodin suppresses hepatocellular carcinoma growth by regulating macrophage polarization via microRNA-26a/transforming growth factor beta 1/protein kinase B. *Bioengineered*. 2022;13(4):9548–9563. doi:10.1080/21655979.2022.2061295
55. Huang J, Yang Y, Zhu Y, et al. DP7-C /mir-26a system promotes bone regeneration by remodeling the osteogenic immune microenvironment. *Oral Dis*. 2024;30(8):5203–5220. doi:10.1111/odi.14910
56. Liu M, Zhang L, Wang T, et al. Application of random number tables in endemic disease surveys[in Chinese]. *Chin j Control End Dis*. 2009;28 (3):351–352.
57. Liu M, Zhao F, Xu J, et al. Qingjin Huatan decoction protects mice against influenza a virus pneumonia via the chemokine signaling pathways. *J Ethnopharmacol*. 2023;317:116745. doi:10.1016/j.jep.2023.116745
58. Qian B, Yang Y, Tang N, et al. M1 macrophage-derived exosomes impair beta cell insulin secretion via miR-212-5p by targeting SIRT2 and inhibiting Akt/GSK-3beta/beta-catenin pathway in mice. *Diabetologia*. 2021;64(9):2037–2051. doi:10.1007/s00125-021-05489-1
59. Assouvie A, Daley-Bauer LP, Rousselet G. Growing murine bone marrow-derived macrophages. *Methods Mol Biol*. 2018;1784:29–33.
60. Coughlan C, Bruce KD, Burgy O, et al. Exosome isolation by ultracentrifugation and precipitation and techniques for downstream analyses. *Curr Protoc Cell Biol*. 2020;88(1):e110. doi:10.1002/cpcb.110
61. Murray CJ, Aravkin AY, Zheng P, et al. Global burden of 87 risk factors in 204 countries and territories, 1990-2019: a systematic analysis for the Global Burden of Disease Study 2019. *Lancet*. 2020;396(10258):1223–1249. doi:10.1016/S0140-6736(20)30752-2
62. Virani SS, Alonso A, Aparicio HJ, et al. Heart disease and stroke statistics-2021 update: a report from the American heart association. *Circulation*. 2021;143(8):e254–e743. doi:10.1161/CIR.0000000000000950
63. Collins R, Reith C, Emberson J, et al. Interpretation of the evidence for the efficacy and safety of statin therapy. *Lancet*. 2016;388 (10059):2532–2561. doi:10.1016/S0140-6736(16)31357-5
64. Fitchett DH, Hegele RA, Verma S. Cardiology patient page. Statin intolerance. *Circulation*. 2015;131(13):e389–91. doi:10.1161/CIRCULATIONAHA.114.013189
65. Wang W, Li H, Shi Y, et al. Targeted intervention of natural medicinal active ingredients and traditional Chinese medicine on epigenetic modification: possible strategies for prevention and treatment of atherosclerosis. *Phytomedicine*. 2024;122:155139. doi:10.1016/j.phymed.2023.155139
66. Zhang M, Liu Y, Xu M, et al. Carotid artery plaque intervention with Tongxinluo capsule (CAPITAL): a multicenter randomized double-blind parallel-group placebo-controlled study. *Sci Rep*. 2019;9(1):4545. doi:10.1038/s41598-019-41118-z
67. Lee B, Han K, Park HJ, et al. Efficacy of Hwangryunhaedok-tang (Huang-lian-jie-du-tang, Oren-gedoku-to) for patients with hyperlipidemia: a study protocol for a randomized, double-blind, placebo-controlled, parallel, investigator-initiated clinical trial. *Trials*. 2020;21(1):750. doi:10.1186/s13063-020-04695-3
68. Luan X, Zhang LJ, Li XQ, et al. Compound-based Chinese medicine formula: from discovery to compatibility mechanism. *J Ethnopharmacol*. 2020;254:112687. doi:10.1016/j.jep.2020.112687
69. Yang Y, Li X, Chen G, et al. Traditional Chinese medicine compound (Tongxinluo) and clinical outcomes of patients with acute myocardial infarction: the CTS-AMI randomized clinical trial. *JAMA*. 2023;330(16):1534–1545. doi:10.1001/jama.2023.19524
70. Johnson J, Carson K, Williams H, et al. Plaque rupture after short periods of fat feeding in the apolipoprotein E-knockout mouse: model characterization and effects of pravastatin treatment. *Circulation*. 2005;111(11):1422–1430. doi:10.1161/01.CIR.0000158435.98035.8D
71. Chen Y, Chen S, Song C, et al. Acute and subchronic toxicity as well as evaluation of safety pharmacology of traditional Chinese medicine "Huhezi". *Int J Clin Exp Med*. 2015;8(8):14553–14564.
72. Kong P, Cui ZY, Huang XF, et al. Inflammation and atherosclerosis: signaling pathways and therapeutic intervention. *Signal Transduct Target Ther*. 2022;7(1):131. doi:10.1038/s41392-022-00955-7
73. Libby P. Inflammation in atherosclerosis. *Nature*. 2002;420(6917):868–874. doi:10.1038/nature01323
74. Zhang Y, Ying F, Tian X, et al. TRPM2 promotes atherosclerotic progression in a mouse model of atherosclerosis. *Cells*. 2022;11(9):1423.
75. Zhang Y, Yang X, Bian F, et al. TNF-alpha promotes early atherosclerosis by increasing transcytosis of LDL across endothelial cells: crosstalk between NF-kappaB and PPAR-gamma. *J Mol Cell Cardiol*. 2014;72:85–94. doi:10.1016/j.yjmcc.2014.02.012
76. Orecchioni M, Wolf D, Suryawanshi V, et al. Deleting interleukin-10 from myeloid cells exacerbates atherosclerosis in Apoe(-/-) mice. *Cell Mol Life Sci*. 2022;80(1):10. doi:10.1007/s00018-022-04649-9
77. Mallat Z, Besnard S, Duriez M, et al. Protective role of interleukin-10 in atherosclerosis. *Circ Res*. 1999;85(8):e17–24. doi:10.1161/01.RES.85.8.e17
78. Libby P, Ridker PM, Hansson GK. Progress and challenges in translating the biology of atherosclerosis. *Nature*. 2011;473(7347):317–325. doi:10.1038/nature10146
79. Fang F, Xiao C, Li C, Liu X, Li S. Tuning macrophages for atherosclerosis treatment. *Regen Biomater*. 2023;10:rbac103. doi:10.1093/rb/rbac103
80. Huang H, Sun Z, Xu J, et al. Yang-Xin-Shu-Mai granule alleviates atherosclerosis by regulating macrophage polarization via the TLR9/MyD88/NF-kappaB signaling pathway. *J Ethnopharmacol*. 2024;318(Pt A):116868. doi:10.1016/j.jep.2023.116868
81. Singh L, Sharma S, Xu S, Tewari D, Fang J. Curcumin as a natural remedy for atherosclerosis: a pharmacological review. *Molecules*. 2021;26 (13):4036. doi:10.3390/molecules26134036
82. Momtazi-Borojeni AA, Abdollahi E, Nikfar B, Chaichian S, Ekhlasi-Hundrieser M. Curcumin as a potential modulator of M1 and M2 macrophages: new insights in atherosclerosis therapy. *Heart Fail Rev*. 2019;24(3):399–409. doi:10.1007/s10741-018-09764-z
83. Capece D, Verzella D, Flati I, et al. NF-kappaB: blending metabolism, immunity, and inflammation. *Trends Immunol*. 2022;43(9):757–775. doi:10.1016/j.it.2022.07.004

84. Wang Y, Zhang J, Yang Z, et al. Ocotillol-type pseudoginsenoside-F11 alleviates lipopolysaccharide-induced acute kidney injury through regulation of macrophage function by suppressing the NF-kappaB/NLRP3/IL-1beta signaling pathway. *J Agric Food Chem*. 2024;72(37):20496–20512. doi:10.1021/acs.jafc.4c05185
85. Liu F, Yang Y, Dong H, et al. Essential oil from Cinnamomum cassia Presl bark regulates macrophage polarization and ameliorates lipopolysaccharide-induced acute lung injury through TLR4/MyD88/NF-kappaB pathway. *Phytomedicine*. 2024;129:155651. doi:10.1016/j.phymed.2024.155651
86. Fang C, Zhong R, Lu S, et al. TREM2 promotes macrophage polarization from M1 to M2 and suppresses osteoarthritis through the NF-kappaB/CXCL3 axis. *Int J Biol Sci*. 2024;20(6):1992–2007. doi:10.7150/ijbs.91519
87. Baeuerle PA, Baltimore D. NF-kappa B: ten years after. *Cell*. 1996;87(1):13–20. doi:10.1016/S0092-8674(00)81318-5
88. Wang D, Tan Z, Yang J, et al. Perfluorooctane sulfonate promotes atherosclerosis by modulating M1 polarization of macrophages through the NF-kappaB pathway. *Ecotoxicol Environ Saf*. 2023;249:114384. doi:10.1016/j.ecoenv.2022.114384
89. Yang S, Li J, Chen Y, et al. MicroRNA-216a promotes M1 macrophages polarization and atherosclerosis progression by activating telomerase via the Smad3/NF-kappaB pathway. *Biochim Biophys Acta Mol Basis Dis*. 2019;1865(7):1772–1781. doi:10.1016/j.bbadis.2018.06.016
90. Zheng Y, Li Y, Ran X, et al. Mettl14 mediates the inflammatory response of macrophages in atherosclerosis through the NF-kappaB/IL-6 signaling pathway. *Cell Mol Life Sci*. 2022;79(6):311. doi:10.1007/s00018-022-04331-0
91. Yunna C, Mengru H, Lei W, Weidong C. Macrophage M1/M2 polarization. *Eur J Pharmacol*. 2020;877:173090. doi:10.1016/j.ejphar.2020.173090
92. Oguz N, Kirca M, Cetin A, Yesilkaya A. Effect of uric acid on inflammatory COX-2 and ROS pathways in vascular smooth muscle cells. *J Recept Signal Transduction Res*. 2017;37(5):500–505. doi:10.1080/10799893.2017.1360350
93. Rumzhum NN, Ammit AJ. Cyclooxygenase 2: its regulation, role and impact in airway inflammation. *Clin Exp Allergy*. 2016;46(3):397–410. doi:10.1111/cea.12697
94. Schonbeck U, Sukhova GK, Graber P, Coulter S, Libby P. Augmented expression of cyclooxygenase-2 in human atherosclerotic lesions. *Am J Pathol*. 1999;155(4):1281–1291. doi:10.1016/S0002-9440(10)65230-3
95. Baker CS, Hall RJ, Evans TJ, et al. Cyclooxygenase-2 is widely expressed in atherosclerotic lesions affecting native and transplanted human coronary arteries and colocalizes with inducible nitric oxide synthase and nitrotyrosine particularly in macrophages. *Arterioscler Thromb Vasc Biol*. 1999;19(3):646–655. doi:10.1161/01.ATV.19.3.646
96. Motino O, Agra N, Brea CR, et al. Cyclooxygenase-2 expression in hepatocytes attenuates non-alcoholic steatohepatitis and liver fibrosis in mice. *Biochim Biophys Acta*. 2016;1862(9):1710–1723. doi:10.1016/j.bbadis.2016.06.009
97. Wang L, Liao Y, Yang R, et al. Sja-miR-71a in Schistosome egg-derived extracellular vesicles suppresses liver fibrosis caused by schistosomiasis via targeting semaphorin 4D. *J Extracell Vesicles*. 2020;9(1):1785738. doi:10.1080/20013078.2020.1785738
98. Li X, Cao Y, Xu X, et al. Sleep deprivation promotes endothelial inflammation and atherogenesis by reducing exosomal miR-182-5p. *Arterioscler Thromb Vasc Biol*. 2023;43(6):995–1014. doi:10.1161/ATVBAHA.123.319026
99. Tang Y, Yang LJ, Liu H, et al. Exosomal miR-27b-3p secreted by visceral adipocytes contributes to endothelial inflammation and atherogenesis. *Cell Rep*. 2023;42(1):111948. doi:10.1016/j.celrep.2022.111948
100. Heo J, Kang H. Exosome-based treatment for atherosclerosis. *Int J Mol Sci*. 2022;23(2):1002. doi:10.3390/ijms23021002
101. Suh JH, Choi E, Cha MJ, et al. Up-regulation of miR-26a promotes apoptosis of hypoxic rat neonatal cardiomyocytes by repressing GSK-3beta protein expression. *Biochem Biophys Res Commun*. 2012;423(2):404–410. doi:10.1016/j.bbrc.2012.05.138
102. Zhang ZH, Li J, Liu BR, et al. MicroRNA-26 was decreased in rat cardiac hypertrophy model and may be a promising therapeutic target. *J Cardiovasc Pharmacol*. 2013;62(3):312–319. doi:10.1097/FJC.0b013e31829b82e6
103. Zhang Y, Qin W, Zhang L, et al. MicroRNA-26a prevents endothelial cell apoptosis by directly targeting TRPC6 in the setting of atherosclerosis. *Sci Rep*. 2015;5:9401. doi:10.1038/srep09401
104. Zhang Z, Gao J, Wang J, et al. Mechanism of zhishi xiebai guizhi decoction to treat atherosclerosis: insights into experiments, network pharmacology and molecular docking. *J Ethnopharmacol*. 2024;333:118466. doi:10.1016/j.jep.2024.118466
105. Wu Z, Wang L, Yin Z, et al. Baoyuan decoction inhibits atherosclerosis progression through suppression peroxidized fatty acid and Src/MKK4/JNK pathway-mediated CD 36 expression. *Phytomedicine*. 2024;130:155668. doi:10.1016/j.phymed.2024.155668
106. Wehbe Z, Wehbe M, Al KA, et al. Emerging understandings of the role of exosomes in atherosclerosis. *J Cell Physiol*;2024. e31454. doi:10.1002/jcp.31454
107. Wang H, Xie Y, Salvador AM, et al. Exosomes: multifaceted messengers in atherosclerosis. *Curr Atheroscler Rep*. 2020;22(10):57. doi:10.1007/s11883-020-00871-7
108. Kamerkar S, LeBleu VS, Sugimoto H, et al. Exosomes facilitate therapeutic targeting of oncogenic KRAS in pancreatic cancer. *Nature*. 2017;546(7659):498–503. doi:10.1038/nature22341

Drug Design, Development and Therapy

Dovepress
Taylor & Francis Group

Publish your work in this journal

Drug Design, Development and Therapy is an international, peer-reviewed open-access journal that spans the spectrum of drug design and development through to clinical applications. Clinical outcomes, patient safety, and programs for the development and effective, safe, and sustained use of medicines are a feature of the journal, which has also been accepted for indexing on PubMed Central. The manuscript management system is completely online and includes a very quick and fair peer-review system, which is all easy to use. Visit http://www.dovepress.com/testimonials.php to read real quotes from published authors.

Submit your manuscript here: https://www.dovepress.com/drug-design-development-and-therapy-journal